

Air Force Institute of Technology

AFIT Scholar

Theses and Dissertations

Student Graduate Works

12-2021

Design and Performance Characterization of a Water Propellant Resistojet Thruster

Sean M. Weathersby

Follow this and additional works at: <https://scholar.afit.edu/etd>



Part of the [Aerospace Engineering Commons](#)

Recommended Citation

Weathersby, Sean M., "Design and Performance Characterization of a Water Propellant Resistojet Thruster" (2021). *Theses and Dissertations*. 5134.

<https://scholar.afit.edu/etd/5134>

This Thesis is brought to you for free and open access by the Student Graduate Works at AFIT Scholar. It has been accepted for inclusion in Theses and Dissertations by an authorized administrator of AFIT Scholar. For more information, please contact AFIT.ENWL.Repository@us.af.mil.



**DESIGN AND PERFORMANCE CHARACTERIZATION OF A WATER-
PROPELLANT RESISTOJET THRUSTER**

THESIS

Sean M. Weathersby, Second Lieutenant, USAF

AFIT-ENY-MS-21-D-077

**DEPARTMENT OF THE AIR FORCE
AIR UNIVERSITY**

AIR FORCE INSTITUTE OF TECHNOLOGY

Wright-Patterson Air Force Base, Ohio

**DISTRIBUTION STATEMENT A.
APPROVED FOR PUBLIC RELEASE; DISTRIBUTION UNLIMITED.**

The views expressed in this thesis are those of the author and do not reflect the official policy or position of the United States Air Force, Department of Defense, or the United States Government. This material is declared a work of the U.S. Government and is not subject to copyright protection in the United States.

AFIT-ENY-MS-21-D-077

DESIGN AND PERFORMANCE CHARACTERIZATION OF A WATER-
PROPELLANT RESISTOJET THRUSTER

THESIS

Presented to the Faculty

Department of Aeronautics and Astronautics

Graduate School of Engineering and Management

Air Force Institute of Technology

Air University

Air Education and Training Command

In Partial Fulfillment of the Requirements for the
Degree of Master of Science in Astronautical Engineering

Sean M. Weathersby, BS

Second Lieutenant, USAF

November 2021

DISTRIBUTION STATEMENT A.
APPROVED FOR PUBLIC RELEASE; DISTRIBUTION UNLIMITED.

AFIT-ENY-MS-21-D-077

DESIGN AND PERFORMANCE CHARACTERIZATION OF A WATER-
PROPELLANT RESISTOJET THRUSTER

Sean M. Weathersby, BS

Second Lieutenant, USAF

Committee Membership:

Dr. Carl Hartsfield
Chair

Dr. Frederick Schauer
Member

Maj Robert Bettinger, PhD
Member

Abstract

Secondary payloads, such as CubeSats, are being increasingly used by the US Department of Defense in the role of defense capability enhancement, and these increasingly complex defense missions can require extended lifespans that result in the need for a thruster. While many thruster options exist, characteristics such as propellant toxicity, complexity, and low performance limit many viable solutions. However, a potential answer that satisfies these thruster limitations is found in electrothermals, specifically the resistojet. The research presented here represents the first attempt to construct a 1U water-propellant resistojet thruster design and establish an initial characterization through evaluation of various performance values and design effects. This was achieved through assembly of additively-manufactured and commercial-off-the-shelf components, as well as construction and use of a vacuum chamber testing bed. This study revealed various inherent assembly risks and design flaws that resulted in the failure of the thruster to enter performance testing, yet heater block functionality was verified and heat loss experimental testing revealed how the design effects result in the propellant tank absorbing detrimental levels of heat over time. Still, due to the rapid function of the heater block, it was determined that this would not pose an operational issue in the future.

I dedicate this body of work to my fiancée, who has chosen selflessly to follow me wherever the wind takes me. This work watched the growth of a scientific idea into a realization, but it also watched the growth of a rekindled relationship into a simple question on Mt. Rainier. With this, my journey of studying the heavens comes to an end, and yet, I cannot wait to continue my journey with you.

Acknowledgements

I would like to thank my research advisor, Dr. Carl Hartsfield, for his unwavering guidance and steadfast support throughout the entirety of this research journey. Truly, the work accomplished in the following pages would not have been possible without his continued counsel and direction every step of the way. Thanks to him, what usually is a perilous, frustrating, and rather intimidating process became an exciting and rewarding journey of hands-on learning. After years of learning countless concepts in textbooks, Dr. Hartsfield allowed me to see them finally come to life, and the lessons I learned along the way were, and will remain, invaluable to my educational career. For that, I am forever grateful. I would also like to thank the lab technicians for their patience and helpfulness, as the numerous requests for assistance were met only with kindness and the willing to lend a hand. Without question, this research would not have been possible without their staunch aid. Finally, I would like to give my sincerest gratitude to the support and encouragement provided by my family and friends throughout this journey. What a gift it is, to be fiercely proud of something, and yet, you come to find that the entirety of those closest to you are proud as well.

Sean M. Weathersby

Table of Contents

	Page
Abstract	iv
Acknowledgements	vi
Table of Contents	vii
List of Figures	ix
List of Tables	xii
I. Introduction	1
Background.....	1
Motivation	7
Research Objectives	7
Scope	8
II. Literature Review	9
Chapter Overview.....	9
Fundamentals of General Rocket Propulsion.....	9
Electrothermal Thrusters and Resistojets	26
Tank Design Considerations.....	36
Small Nozzle Effects	39
Radiative Heat Transfer Considerations.....	41
Summary.....	46
III. Methodology	48
Chapter Overview.....	48
Thruster Design	48
Assembly and Integration.....	54
Experimental Testing.....	79

Data Reduction	84
Data Uncertainty and Experimental Error	84
Expected Performance Results	85
IV. Analysis and Results	89
Chapter Overview	89
Results of Thruster Assembly and Integration	89
Results of Heater Block Functional Check	97
Results of Resistor Component Heat Losses	98
V. Conclusions and Recommendations	106
Chapter Overview	106
Conclusions of Research	106
Significance of Research	107
Recommendations for Action	108
Recommendations for Future Research	109
Appendix A: Open Chamber Experiment Data Table	110
Appendix B: Closed Chamber Experiment Data Table	113
Bibliography	116

List of Figures

	Page
Figure 1. Rocket Free-Body Diagram derived from lecture on Advanced Rocket Propulsion by Arif Karabeyoglu of Stanford University	15
Figure 2. Converging-Diverging Nozzle [13].....	23
Figure 3. Conceptual Model of Electrothermal Thruster derived from Physics of Electric Propulsion by Robert G. Jahn	27
Figure 4. Vapor Pressure Dependency of R-236fa with respect to temperature [19].....	38
Figure 5. LBPF Nozzle Topography [20].....	41
Figure 6. Propellant Control Valve Design.....	51
Figure 7. Computer Aided Design of Thruster System Layout [19]	54
Figure 8. Initial Setup of Vacuum Chamber Facility.....	55
Figure 9. Thermocouple Flange.....	56
Figure 10. Canon Plug Flange	56
Figure 11. External Wiring Harness	57
Figure 12. Load Cell Flange	58
Figure 13. Initial Build of Instrument Bed.....	59
Figure 14. 3D Printed Adapter.....	59
Figure 15. External Terminal Board Interface	60
Figure 16. Internal Terminal Board Interface	61
Figure 17. Adjusted Thrust Stand Adapter	62
Figure 18. Thruster Adjustments	64
Figure 19. Water-Propellant Resistojet Thruster	69

Figure 20. Wired Internal Instrument Board.....	70
Figure 21. Thermocouple Wiring and Pressurant Hookup	71
Figure 22. Controller Setup.....	72
Figure 23. Switch Box Interior	73
Figure 24. Switch Box Setup	73
Figure 25. External Wiring	74
Figure 26. External Power Supplies.....	75
Figure 27. Data Acquisition Board Setup.....	75
Figure 28. Vacuum Chamber Sensor	76
Figure 29. External Instrument Setup	76
Figure 30. External Gas Tank Setup	77
Figure 31. Additional Relay Set.....	77
Figure 32. Temperature Reading Setup	80
Figure 33. Heat Loss Experiment Setup	82
Figure 34. Thruster in Testing	82
Figure 35. Tank and Valve System Bypass	83
Figure 36. Expected Thrust Performance of Resistojet Thruster [19].....	86
Figure 37. Expected Specific Impulse Performance of Resistojet Thruster [19]	87
Figure 38. Control Valve Installation Failure	91
Figure 39. Corrective Control Valve	91
Figure 40. Teflon Tape Sealing	93
Figure 41. Corrective RTV Sealing	93
Figure 42. Corrective RTV Sealing	94

Figure 43. Installed Valve Manifold.....	96
Figure 44. Epoxy Application.....	96
Figure 45. Observable Thrust	97
Figure 46. Heater Block Enthalpy Curves	100
Figure 47. Tank Temperature	101
Figure 48. Initial Heater Block Temperature	102

List of Tables

	Page
Table 1. Emissivity Values of Inconel 718 [22]	44
Table 2. Absorptivity Values of AlSi12 Aluminum Alloy [23]	45

DESIGN AND PERFORMANCE CHARACTERIZATION OF A WATER- PROPELLANT RESISTOJET THRUSTER

I. Introduction

Background

The standard payload structure for current space launches consists of a primary payload as well as additional secondary payloads. NASA has defined these payload classifications in past policy outlines for cases of excess launch vehicle capacity, where a primary payload is one that “drives the overall mission launch schedule and orbital trajectory and is responsible for the costs associated with the launch service”. [1] A secondary payload is then defined as “an experiment, sensor, instrument or fully integrated payload whose mission objective is different than that of the primary payload mission objective”. [1] This infers the question of why secondary payloads exist at all, as tailoring a payload mission design to fit the needs of another is not ideal for any program.

Often times universities, scientific institutes, private companies, and other organizations do not have the financial resources to fully fund a lift to orbit from a launch agency, and thus the alternative is to “catch a ride” on an already upcoming launch. For such cases, the required payload orbit can be flexible and is more focused on achieving access to space in general. If possible then, the logical step for a launch agency is to carry additional, secondary payloads to provide a relatively low-cost spaceflight opportunity for smaller experiments, instruments, or satellites, sometimes at no cost or at a fraction of the launch service costs. [1]

Still, it is the success of the primary payload that takes precedence over the success of the secondary payloads, as it is the future operator of this primary payload that is the primary customer of the launch agency, who provides the lift to orbit. Thus, the primary payload users can have varying authority with regards to the integration and initial operation procedures of the secondary payloads. Success of the primary payload can also include the successful security of classified technology, and to protect national security interests the Department of Defense (DoD) can have authority on which secondary payloads, if any, may launch on DoD spaceflights. [1]

However, this authority by the primary payload user remains even where the primary payload is a private or commercial interest, and the protection of classified technology is not an issue. In these cases, as well as all cases of excess launch vehicle capacity, the inclusion of secondary payloads becomes a matter of safety, and certain measures are taken to ensure any secondary payloads do not pose a threat to the successful deployment and operation of the primary payload. While restrictions can be put on secondary payloads that are not particularly difficult to meet, sometimes if a secondary payload is deemed enough of a risk to the success of the primary payload, it can be denied the opportunity to receive a launch slot entirely. A more intuitive thought process would be that the launch agency holds the authority for what launches, but in fact it is the primary payload mission director that “retains the final authority to allow or disallow launch of a [secondary] payload”. [1]

Even with the disadvantages that come with the classification of a secondary payload, this has not stopped the growth of the small satellite market within the past decades. During the 1990s the US options for a secondary payload rideshare mainly

centered around the NASA Space Shuttle and various expendable launch vehicles. [1] Since then, technological advancements have allowed for more efficient and cost-effective integration of secondary payloads as well as a massive reduction in overall launch costs. The ESPA ring, or the Evolved Expendable Launch Vehicle Secondary Payload Adapter, has been the prime example of this more cost-effective integration. Fitted with bolt interfaces as a drop-in component in the launch stack, the ESPA ring utilizes excess launch capacity by fitting secondary payloads below the primary spacecraft. The ESPA ring has allowed for the easy inclusion of secondary payloads with a minimal impact to the primary payload, increasing overall safety. The resulting reduction in launch costs brought by the ESPA ring has made it an industry standard for small satellite adapters. [2]

While secondary payload integration advancements have made an observable impact, arguably the other largest contribution towards the growth in the small satellite market is the recent development of the reusable launch vehicle. The prime example of this development is found in the rockets used by SpaceX. With the introduction of the Falcon 9, it became the first ever orbital-class rocket that is reusable. This reusability allows for the most expensive parts of the rocket to be re-flown, thus driving down the total cost of space access. [3] This reduction in cost has not just been incremental, and in fact has been a reduction by over an order of magnitude. While the NASA space shuttle had a cost of roughly \$54,500 per kilogram to launch to low-earth orbit, the SpaceX Falcon 9 accomplishes the same for only \$2,720 per kilogram. [4] Reducing this total launch cost allows for an easier access to space by institutes, companies, and universities, thereby boosting the presence of small satellites in the current space industry.

The skyrocketed presence of small satellites in the space industry even resulted in SpaceX developing a dedicated rideshare program for secondary payloads. In March 2014, the company suggested that there would still be a presence of secondary payloads within their launches, but there would not be many, as they did not see a large market for secondary payloads at the time. [5] Several years later, in August 2019 SpaceX made a stark change from this view when they announced a dedicated rideshare program for small satellites on their future launches, offering reduced prices and increased launch opportunities. [6] This growth in the industry presence of small satellites shows no sign of stopping, as the small satellite market was valued at \$3,632.4 million in 2018 and is projected to reach a market value of \$15,686.3 million by 2026. [7]

Still, while the small satellite market is experiencing rapid growth in the commercial sector, the fact remains that on launches where the Department of Defense is the primary payload user, they have the authority to deny rideshare for commercial secondary payloads. This leads to an inquiry of what DoD secondary payloads are taking the place of these commercial payload absences, how significant is their presence, and what DoD missions are even viable using just secondary payloads. While in the past the Department of Defense has focused mainly on large, primary payloads, it has been found that small satellites, such as CubeSats, are “increasingly being used by defense organizations globally to improve the battlefield communications, gather information from unattended sensors, and monitor space weather”. [7] Additional defense sector applications of these small satellites include medium resolution imagery, tactical communication, as well as geospatial and atmospheric research. [7]

Even if the secondary payloads on a launch come from various organizations within the DoD itself, there is still priority that remains with the success of the primary payload. Therefore, the restrictions that can be placed on secondary payloads still apply, and can drive many decisions in the engineering design process for these small satellites. With the decreasing costs of launching secondary payloads and their increasing use in defense applications, there has never been a better time for DoD organizations to develop small satellites to achieve various objectives, providing that this can be done under the restrictions set by primary payloads. Thus, an incentive is provided to the manufacturers of secondary payloads to design a payload that is easy to integrate within the launch vehicle, safe, reliable, predictable, and overall low-risk to the success of the primary payload.

This authority held by the primary payload user can even extend to the initial operation procedures of the secondary payloads, such as deployment from the launch vehicle. In some cases, these small satellites are deployed early as to not interfere with the deployment of the primary payload. Alternatively, the secondary payloads can be deployed late, as this accomplishes the same objective of preventing interference due to the booster having descended back to a lower altitude. While this method does prevent interference with the deployment of the primary payload, another issue arises. At lower altitudes, these small satellites are more subject to the effects of atmospheric drag. As the satellite continues to orbit, atmospheric drag lowers the altitude of the orbit itself, until eventually the satellite enters a re-entry trajectory and is burned up in the atmosphere.

While this may be standard for certain small satellites, where the mission lifetime was planned to be relatively short and the satellite was coordinated to be disposed of in

re-entry, this is not the case for many small satellites. As mentioned, small satellites are finding use in increasingly complex defense missions, and can thus require extended lifespans, more than just the initial orbit alone can provide. This introduces the need for thrusters that can accomplish such a lifespan extension. Many small thrusters exist today that perform various mission needs and span a wide array of technologies, including monopropellant thrusters, electrostatic thrusters, and cold gas thrusters. However, not all small thrusters fit the needs of every mission, and sometimes if a thruster does meet a mission need, its design or operation can violate restrictions set by a primary payload.

For instance, hydrazine monopropellant thrusters are common in use for on-orbit spacecraft. The hydrazine monopropellant is stable, storable, simple, and has a high specific impulse, allowing it to meet many orbit maintenance needs. However, hydrazine is also extremely toxic and therefore difficult to work with, allowing the potential for dangerous effects if something were to go wrong. [8] Because of this, a primary payload user may restrict the use of such a monopropellant by other payloads, and while this thruster is still high performance and meets mission needs, it is no longer viable. On the other hand, thrusters such as electrostatics are complex and thus more prone to unreliability. Additionally, while electrostatic thrusters do have a relatively high Isp, they can sometimes not provide the thrust required to perform adequate orbit maintenance for certain missions. Even if the complexity issue is removed by using a cold gas thruster, the performance of this thruster can still not be high enough for use in orbit maintenance, and is instead more practical in the role of attitude control. While these thrusters and more are not suitable for certain orbit maintenance missions, a solution does exist. The answer to this problem is found in the use of electrothermal thrusters, such as the resistojet.

Motivation

With small satellites being used in more complex defense missions, the Air Force Institute of Technology has been performing small thruster research in the search to find solutions to increasing the lifespan of DoD secondary payloads. While AFIT has done research in the past with electrostatics, testing found that these thrusters did not have a high level of performance. [9] Thus, AFIT has moved to begin research into electrothermal thrusters with propellants suitable for secondary payloads. Specifically, water as a propellant holds a major advantage in that it is non-toxic, and can thus be used when a primary payload puts restrictions on toxic propellants for secondary payloads. Furthermore, water has already been proven viable to be used directly as a propellant, in both steam and plasma. [10] Following, AFIT has sent a proposal to a government sponsor for a water-propellant resistojet thruster design, which has since been funded. There is now a desire to characterize this thruster, evaluating various performance values and design effects.

Research Objectives

The primary research objective is to evaluate different performance values and design effects of a water-propellant resistojet thruster when subject to varying testing conditions. Performance values that cannot be directly evaluated from test results should be calculated using thermodynamic relations with performance values that can be directly measured. The specific design effects to be analyzed are the heat losses that occur from the resistor component of the thruster.

Scope

The scope of this research is focused on evaluating different thruster performance values and thruster design effects through testing within a laboratory environment.

Performance testing conditions will change to reflect the different thrust modes that are used in various spaceflight missions, such as short pulses and extended duration pulses.

Further performance testing will then lead to evaluation of thruster limits and requirements. Testing of design effects will focus on the mechanisms and results of any heat losses originating from the thruster resistor component, specifically with regards to effects felt by the thruster propellant tank.

II. Literature Review

Chapter Overview

The purpose of this chapter is to discuss the fundamentals of general rocket propulsion, concepts of electrothermal propulsion and resistojets, associated methods of heat transfer analysis, various tank design considerations, effects of small nozzles, and different radiative heat transfer considerations. This chapter includes existing literature for previous work that has been conducted on adjacent topics. The concepts discussed in this chapter will be referenced and applied in following chapters.

Fundamentals of General Rocket Propulsion

At the most basic level, propulsion is defined as “the act of changing the motion of a body with respect to an inertial reference frame”. [11, p. 1] Still, this definition is quite broad, and thus the term jet propulsion is defined as “a type of motion whereby a reaction force is imparted to a vehicle by the momentum of ejected matter”. [11, p. 1] This definition more suits the purposes of space travel, but does not quite fully narrow in. While both air-breathing vehicles and rockets accomplish motion through jet propulsion, the difference is that with rocket propulsion, all of the ejected matter is stored within the vehicle itself. Regardless of the exact method for achieving this, this idea is fundamental to all rocket propulsion thrusters.

Due to this shared idea that ejected propellant can impart a momentum change, and thus a propulsive force, it follows that all rocket propulsion thrusters can be evaluated on how well this is achieved. While many different thrusters exist and the methods to create a propulsive force can vary widely, all share the need for certain

measures that evaluate performance. Perhaps the most basic measure of performance of a rocket is evaluating how much total energy the rocket and its propellant can provide. This is also known as the total impulse, and is found by integrating the thrust force over the time of its application. [11, p. 26] It is defined below in Equation 1.

$$I_t = \int_0^t F dt \quad (1)$$

where:

$$I_t = \text{total impulse [N} \cdot \text{sec]}$$

$$F = \text{thrust [N]}$$

$$t = \text{time [sec]}$$

For constant thrust, where there are assumed negligibly short start and stop transients, the definition for total impulse can be reduced, as seen in Equation 2. [11, p. 26]

$$I_t = Ft \quad (2)$$

It is important to note that this assumption cannot always be made when evaluating rocket propulsion thrusters, and in many cases the start and stop transients can have a sizeable effect on the performance.

Another measure of performance that is quite useful in the analysis of a thruster is the specific impulse, which is defined as the thrust per unit propellant weight flow rate. [11, p. 27] The mathematical definition for specific impulse is given in Equation 3 below.

$$I_{sp} = \frac{\int_0^t F dt}{g_0 \int_0^t \dot{m} dt} \quad (3)$$

where:

$$I_{sp} = \text{specific impulse [sec]}$$

$$F = \text{thrust [N]}$$

$$g_0 = \text{standard acceleration of gravity } \left[\frac{m}{sec^2} \right]$$

$$\dot{m} = \text{total propellant mass flow rate } \left[\frac{kg}{sec} \right]$$

$$t = \text{time [sec]}$$

Upon close inspection, it is seen that the term in the numerator is just total impulse, which has been previously defined. Furthermore, since the integral in the denominator is the mass flow rate integrated over a specified time of propellant ejection, it can be redefined as the total effective propellant mass expelled. Thus, specific impulse can also be defined as shown in Equation 4.

$$I_{sp} = \frac{I_t}{m_p g_0} \quad (4)$$

where:

$$I_{sp} = \text{specific impulse [sec]}$$

$$I_t = \text{total impulse [N} \cdot \text{sec]}$$

$$g_0 = \text{standard acceleration of gravity } \left[\frac{m}{sec^2} \right]$$

$$m_p = \text{total effective propellant mass expelled [kg]}$$

Similar to the reductions made previously, if propellant mass flow and thrust are held constant and transients are assumed negligible, specific impulse is reduced as shown in Equation 5. [11, p. 27]

$$I_{sp} = \frac{F}{\dot{m} g_0} = \frac{F}{\dot{w}} = \frac{I_t}{w} \quad (5)$$

Where w is *weight* and \dot{w} is the *weight flow rate*. Again, this reduction does not hold viable in cases of significant transient effects, where performance can be considerably impacted.

Specific impulse is an important measure of performance, as it evaluates how well a rocket propulsion thruster can convert propellant mass to a propulsive force. While the units of seconds seems unintuitive, it is providing the information of how long a rocket could produce 1 unit force of thrust if given 1 unit weight of propellant. When looking at the definition of specific impulse, an initial glance might lead to the idea that it is a measure of efficiency, but this would be incorrect. Efficiencies do not have units, and specific impulse is instead a performance rating, which does have units. A similar concept to specific impulse that applies to automobiles would be the performance measure of miles per gallon. [11, p. 27]

From specific impulse, there is another performance measure that is used when evaluating exhaust velocity of a thruster. It is called effective exhaust velocity, and is defined below in Equation 6.

$$c = I_{sp}g_0 = \frac{F}{\dot{m}} \quad (6)$$

Where c is the *effective exhaust velocity* and is related to previously defined parameters. Effective exhaust velocity measures the mass-equivalent or average velocity at which propellant mass is ejected from the thruster itself. It is useful in that rocket nozzles typically do not have a uniform exhaust velocity profile over the exit cross section and is thus difficult to accurately measure. Instead, this performance measure is used as a

substitute for a uniform axial velocity. Since specific impulse and effective exhaust velocity are related by a constant, they are often used interchangeably. [11, pp. 27-28]

While thrust has been mentioned in defining previous performance measures, it is itself a performance measure, and one of the most important measures at that. Even though certain thrusters may not have a high level of thrust themselves, their fundamental purpose is still to provide thrust to the vehicle. Thrust directly relates to the definition of rocket propulsion as outlined previously, where internally stored ejected matter imparts a momentum change leading to a propulsive force; this propulsive force is thrust. The thrust produced by a rocket due to this imparted momentum change is then defined as below in Equation 7.

$$F = \frac{d(mv_2)}{dt} = \dot{m}v_2 \quad (7)$$

where:

$$F = \text{thrust [N]}$$

$$m = \text{ejected propellant mass [kg]}$$

$$\dot{m} = \text{mass flow rate } \left[\frac{\text{kg}}{\text{sec}}\right]$$

$$v_2 = \text{exit gas velocity } \left[\frac{\text{m}}{\text{sec}}\right]$$

While this is the concept of thrust defined in the simplest form, a number of assumptions have been made. Here, the exit gas velocity is assumed to be constant, as well as uniform and purely axial. Additionally, this definition of thrust only applies when the pressure of the nozzle exit is equal to the surrounding ambient pressure. [11, p. 32]

As altitude changes with flight, there are variations in the surrounding ambient pressure due to atmospheric density decreasing with height. This results in an imbalance between this ambient pressure and the propellant gas pressure at the nozzle exit plane. This pressure imbalance creates a second component of thrust alongside the thrust due to an imparted momentum change. This full thrust equation is given below in Equation 8.

$$F = \dot{m}v_2 + (p_2 - p_3)A_2 \quad (8)$$

where:

$$F = \text{thrust [N]}$$

$$\dot{m} = \text{mass flow rate } \left[\frac{\text{kg}}{\text{sec}}\right]$$

$$v_2 = \text{exit gas velocity } \left[\frac{\text{m}}{\text{sec}}\right]$$

$$p_2 = \text{gas pressure at the exit [Pa]}$$

$$p_3 = \text{ambient pressure [Pa]}$$

$$A_2 = \text{nozzle exit cross sectional area [m}^2\text{]}$$

In this equation for thrust, the two components added are defined as the momentum thrust and the pressure thrust, respectively. In the case where the surrounding ambient pressure is greater than the exit gas pressure, the pressure thrust term becomes negative and leads to a lower overall thrust. When the two pressure values are equal, the thrust equation reverts to as shown in Equation 7. [11, pp. 32-33]

Most often though, the pressure thrust term is some positive value and adds to the overall thrust. There is a limit to this, and it is represented below in Equation 9.

$$F = \dot{m}v_2 + p_2A_2 \quad (9)$$

When the surrounding ambient pressure reaches a value of 0, the thrust equation reduces to as shown. Here, the pressure thrust term is at a maximum value. This reduction is important because it occurs where ambient pressure is nonexistent, in other words, the vacuum of space. [11, p. 33]

To fully understand thrust as a performance measure and the relationship it has with a rocket propulsion system, it is important to look at the derivation it has beginning from a simple force balance of the rocket. As a visual reference, the free body diagram for a typical rocket is given below in Figure 1.

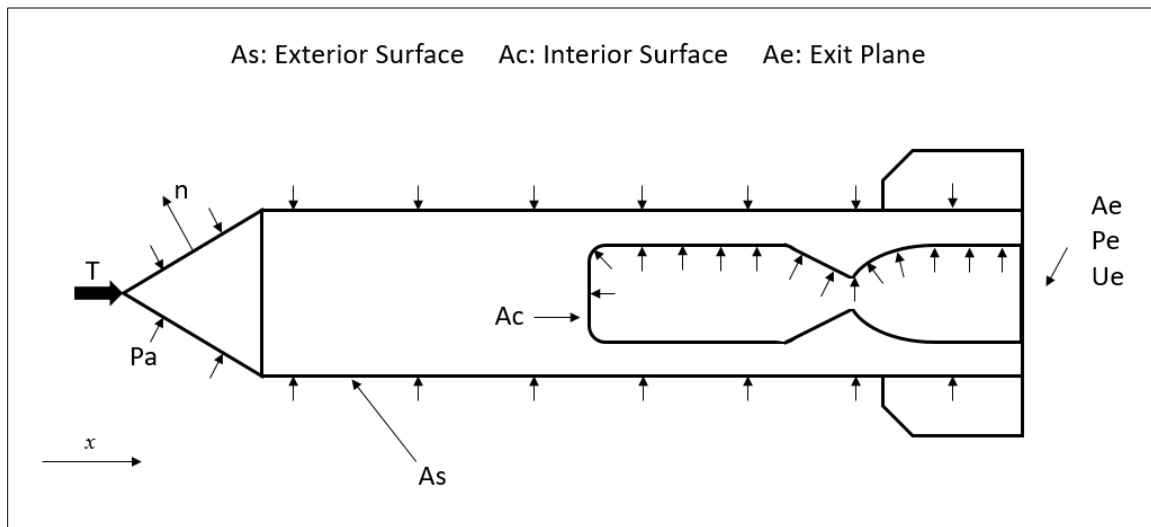


Figure 1. Rocket Free-Body Diagram derived from lecture on Advanced Rocket Propulsion by Arif Karabeyoglu of Stanford University

Assume all external gas is at rest and no body forces are acting on the rocket, and perform a force balance.

$$T + \int_{A_s} P_a \hat{n} dA + \int_{A_c} (P\bar{I} - \bar{\tau}) \cdot \hat{n} dA = 0 \quad (10)$$

Where \bar{I} is a *unity tensor*, $\bar{\tau}$ is a *stress tensor*, P is *pressure*, P_a is *ambient pressure*, T is the *thrust force*, and both integrals are performed over the defined x direction. Then, for the first integral identify that $A_s + A_c$ and $A_c + A_e$ are closed surfaces and P_a is constant.

$$\int_{A_s+A_c} P_a \hat{n} dA = 0 \quad (11)$$

$$\int_{A_c+A_e} P_a \hat{n} dA = 0 \quad (12)$$

Separate and combine to yield a simplified expression for the first integral term.

$$\int_{A_s} P_a \hat{n} dA = P_a A_e \quad (13)$$

Develop the second integral term by assuming no body forces act on the working gas, and state the momentum equation.

$$\frac{\partial \rho \bar{u}}{\partial t} + \nabla \cdot (\rho \bar{u} \bar{u} + P\bar{I} - \bar{\tau}) = 0 \quad (14)$$

Where \bar{u} is the *velocity vector* and ρ is the *density*. Then, assume a quasi-steady operation and define a control volume as covered by $A_c + A_e$. Assume that the control volume is constant with time, and take the integral of the momentum equation over the control volume.

$$\int_{cv} \nabla \cdot (\rho \bar{u} \bar{u} + P\bar{I} - \bar{\tau}) dv = 0 \quad (15)$$

Implement Gauss's Theorem and obtain an expanded expression.

$$\int_{A_c} (\rho \bar{u} \bar{u} + P \bar{I} - \bar{\tau}) \cdot \hat{n} dA + \int_{A_e} (\rho \bar{u} \bar{u} + P \bar{I} - \bar{\tau}) \cdot \hat{n} dA = 0 \quad (16)$$

Apply a no slip condition in the defined x direction.

$$\int_{A_c} (P \bar{I} - \bar{\tau}) \cdot \hat{n} dA + \rho_e u_e^2 A_e + P_e A_e = 0 \quad (17)$$

$$\int_{A_c} (P \bar{I} - \bar{\tau}) \cdot \hat{n} dA = -\rho_e u_e^2 A_e - P_e A_e \quad (18)$$

Where there is assumed quasi-one-dimensional flow at nozzle exit, ignored higher order terms, average quantities have been introduced at exit plane, and an assumption made of the stress tensor, which is shown below.

$$\int_{A_e} \bar{\tau} \cdot \hat{n} dA \cong 0 \quad (19)$$

Combine to obtain an expression for the thrust force.

$$T = \rho_e u_e^2 A_e + (P_e - P_a) A_e \quad (20)$$

Define mass flow rate, substitute, and arrive at a final expression for thrust.

$$\dot{m} = \rho_e u_e A_e \quad (21)$$

$$T = \dot{m} u_e + (P_e - P_a) A_e \quad (22)$$

It should be noted that this derivation represents certain variables differently than the thrust equation given in Equation 8, but there is no difference in terms of modeling the thrust produced by a rocket. [12]

Since rocket vehicles operate on this idea of thrust and ejecting mass to push mass, it is useful to have a measure of how the propellant mass and the mass of the vehicle alone are related. This is accomplished using the performance measures of mass

ratio and propellant mass fraction, which are defined below in Equation 23 and Equation 24, respectively. [11, pp. 28-29]

$$MR = \frac{m_f}{m_0} \quad (23)$$

where: $MR = \text{mass ratio [unitless]}$

$m_f = \text{vehicle mass after total propellant ejection [kg]}$

$m_0 = \text{initial vehicle mass [kg]}$

$$\zeta = \frac{m_p}{m_0} \quad (24)$$

where: $\zeta = \text{propellant mass fraction [unitless]}$

$m_0 = \text{initial vehicle mass [kg]}$

$m_p = \text{total effective propellant mass [kg]}$

Typically, it is desired to have a smaller inert mass and have the propellant mass be a larger portion of the total initial vehicle mass. This is because as propellant is ejected, the rocket hardware attempting to accelerate will be able to do so easier than a vehicle where the hardware itself takes up a higher portion of the total mass.

While mass ratio and propellant fraction are intuitively derived values and simply just fractions, concepts such as specific impulse and thrust have holdings in thermodynamic theory, at least for rocket thrusters that operate off thermodynamic gas expansion. While several performance measures have been defined thus far, there are additional measures of performance that can effectively characterize a thruster and aid in design considerations. These performance measures apply mainly for certain thermal

rocket propulsion systems, and thus arise from application of thermodynamics.

Therefore, they require a brief discussion of thermodynamic theory and nozzle flow.

In order to obtain these performance measures, an assumption must be made that the rocket propulsion system is an ideal system. This allows for the reduction of the multi-dimensional equations of aerothermochemical behavior into simple mathematical relationships. The assumptions that accompany an ideal rocket propulsion system are listed below, taken directly from *Rocket Propulsion Elements* by Sutton and Biblarz.

- “The working fluid is homogeneous in composition.” [11, p. 46]
- “All the species of the working fluid are treated as gaseous. Any condensed phases add a negligible amount to the total mass.” [11, p. 46]
- “The working fluid obeys the perfect gas law.” [11, p. 46]
- “There is no heat transfer across any and all gas-enclosure walls; therefore, the flow is adiabatic.” [11, p. 46]
- “There is no appreciable wall friction and all boundary layer effects may be neglected.” [11, p. 46]
- “There are no shock waves or other discontinuities within the nozzle flow.” [11, p. 46]
- “The propellant flow rate is steady and constant. The expansion of the working fluid is uniform and steady, without gas pulsations or significant turbulence.” [11, p. 46]
- “Transient effects are of such short duration that they may be neglected.”
- “All exhaust gases leaving the rocket nozzles travel with a velocity parallel to the nozzle axis.” [11, p. 46]

- “The gas velocity, pressure, temperature, and density are all uniform across any section normal to the nozzle axis.” [11, p. 46]
- “Chemical equilibrium is established within the preceding combustion chamber and gas composition does not change in the nozzle.” [11, p. 46]
- “Ordinary propellants are stored at ambient temperatures. Cryogenic propellants are at their boiling points.” [11, p. 46]

These assumptions allow for the derivation of simplified thermodynamic relations, leading to useful performance measures for rocket thrusters. While the assumptions that come with an ideal rocket propulsion system do not always hold valid, they are quite useful for preliminary design with appropriate corrections made afterwards. [11, p. 46]

In the development of these relations, certain fundamental principles are necessary to be applied to the processes inside the thruster. Some of these include the principles of conservation of energy, conservation of mass, perfect gas law, and isentropic flow. Perhaps the most visible of these is the principle of isentropic flow, as it holds a significant role in the development of certain performance measures. The isentropic flow equations are shown below in Equation 25.

$$\frac{T_x}{T_y} = \frac{P_x}{P_y} \frac{(\gamma-1)}{\gamma} = \frac{V_y^{\gamma-1}}{V_x^{\gamma-1}} \quad (25)$$

where:

$T = \text{temperature [K]}$

$P = \text{pressure [Pa]}$

$V = \text{volume [m}^3\text{]}$

$\gamma = \text{ratio of specific heats [unitless]}$

$x = \text{arbitrary position in nozzle}$

$y = \text{separate arbitrary position in nozzle}$

These equations are quite useful, as they show the relationship of various properties between any two points within a rocket nozzle. The concept of isentropic flow results from the assumptions made of ideal rocket propulsion systems, and define a flow that is of constant entropy; the thermodynamic process of isentropic flow is both adiabatic and reversible. [11, pp. 47-48]

These flow equations can be applied in concert with the principle of conservation of energy and the relationship it has with change in static enthalpy to get a simplified expression for the exit gas velocity. Further development of this expression alongside certain concepts of Mach number and stagnation values lead to substitutions that can be made in previously defined equations for thrust. Further rearrangement then brings the arrival of a new performance measure that assesses the effects of the nozzle of a rocket on the performance and is known as the thrust coefficient, or C_F . The definition for C_F is given below in Equation 26. [11, pp. 48-62]

$$C_F = \sqrt{\frac{2\gamma^2}{\gamma-1} \left(\frac{2}{\gamma+1}\right)^{\frac{\gamma+1}{\gamma-1}} \left[1 - \left(\frac{p_2}{p_1}\right)^{\frac{\gamma-1}{\gamma}}\right]} + \frac{p_2 - p_3}{p_1} \frac{A_2}{A_t} \quad (26)$$

where:

$C_F = \text{thrust coefficient [unitless]}$

$\gamma = \text{ratio of specific heats [unitless]}$

$p_1 = \text{chamber pressure [Pa]}$

$p_2 = \text{pressure at nozzle exit plane [Pa]}$

$$p_3 = \text{ambient pressure [Pa]}$$

$$A_t = \text{nozzle throat cross sectional area [m}^2\text{]}$$

$$A_2 = \text{nozzle exit cross sectional area [m}^2\text{]}$$

The thrust coefficient C_F can then also be defined in terms of thrust, a previously defined performance measure. This is shown below in Equation 27.

$$C_F = \frac{F}{p_1 A_t} \quad (27)$$

Where all present variables have been previously defined. The thrust coefficient of a rocket propulsion system is quite useful as a performance measure, as it represents the amplification of the thrust due to the expansion of the gas in the diverging section of the converging-diverging nozzle compared to the thrust that would be measured if the chamber pressure exerted force over the nozzle throat area alone. It is also convenient for use in visualizing the effects of variations in chamber pressure and altitude for certain nozzle configurations. [11, pp. 62-63] As a visual reference for understanding thrust coefficient, a diagram of a typical converging-diverging nozzle used in modern rocket vehicles is given below in Figure 2.

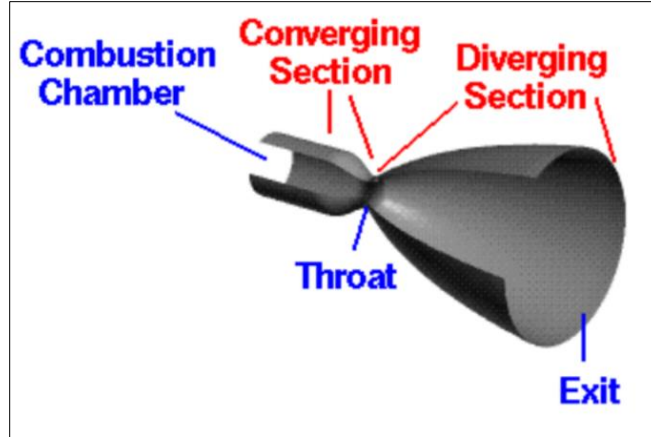


Figure 2. Converging-Diverging Nozzle [13]

Manipulating previously defined performance measures together can give new and useful measures of performance that aid in analysis of a rocket propulsion system. In contrast to thrust coefficient, which measured nozzle effects, a performance measure used often when assessing the performance separate from nozzle effects is the characteristic velocity, or c^* . It can be found by relating the previously defined performance measures of effective exhaust velocity and thrust coefficient, and is defined below in Equation 28. [11, p. 63]

$$c^* = \frac{c}{C_F} = \frac{I_{sp}g_0}{C_F} = \frac{\sqrt{\gamma RT_1}}{\gamma \sqrt{\left[\frac{2}{\gamma+1}\right]^{\frac{\gamma+1}{\gamma}}}} \quad (28)$$

where:

$c^* = \text{characteristic velocity } \left[\frac{m}{s}\right]$

$c = \text{effective exhaust velocity } \left[\frac{m}{s}\right]$

$C_F = \text{thrust coefficient [unitless]}$

$T_1 = \text{chamber temperature [K]}$

Characteristic velocity can also then be defined using other various measurements if the previous performance measures are not readily available. This is shown below in Equation 29.

$$c^* = \frac{p_1 A_t}{\dot{m}} \quad (29)$$

While stated as a velocity with units of meters per second, characteristic velocity is not a physical velocity. It is used as a measure of performance of the propulsion system design and the propellants; in chemical rockets it is closely related to the efficiency of the combustion process. Because this performance measure is a function of propulsion system properties and propellant properties only, it is essentially independent of nozzle characteristics. This allows for the convenience of thruster analysis separate from the nozzle. [11, pp. 34, 63]

With the definition of these performance measures, there can now be a derivation of an expression for the maximum attainable flight velocity increment in a gravity-free vacuum. Begin with Newton's Second Law of Motion for a vehicle with an instantaneous mass.

$$F = m \frac{dv}{dt} \quad (30)$$

Where m is this *instantaneous mass* and v is the *flight velocity*. Assume startup and shutdown durations can be neglected and manifest an expression for the instantaneous mass of the vehicle as a function of time.

$$m = m_0 - \frac{m_p}{t_p} t = m_0 \left(1 - \frac{m_p}{m_0} \frac{t}{t_p} \right) \quad (31)$$

$$m = m_0 \left(1 - \zeta \frac{t}{t_p} \right) = m_0 \left[1 - (1 - MR) \frac{t}{t_p} \right] \quad (32)$$

Where m_0 is the *initial mass of the vehicle*, m_p is the *initial propellant mass*, t_p is the *time at power cutoff* and the performance measures ζ and MR have been previously defined. Rearrange Equation 30 and substitute in previously defined performance measures.

$$dv = \left(\frac{F}{m}\right) dt = \left(\frac{c\dot{m}}{m}\right) dt \quad (33)$$

$$dv = \frac{(c\dot{m})dt}{m_0 - \frac{m_p t}{t_p}} = \frac{c \left(\frac{m_p}{t_p}\right) dt}{m_0 \left(1 - \frac{m_p t}{m_0 t_p}\right)} = c \frac{d\left(\frac{\zeta t}{t_p}\right)}{1 - \frac{\zeta t}{t_p}} \quad (34)$$

Integrate and identify that the frame of reference will not always give a zero initial velocity, represent instead as a velocity increment.

$$\Delta v = -c \ln(1 - \zeta) + v_0 = c \ln\left(\frac{m_0}{m_f}\right) + v_0 \quad (35)$$

Substitute in definitions for previously defined performance measures and arrive at a final expression.

$$\Delta v = I_{sp} g_0 \ln\left(\frac{m_0}{m_f}\right) + v_0 \quad (36)$$

This expression is known as the Tsiolkovsky rocket equation, or the ideal rocket equation. It is one of the fundamental equations of general rocket propulsion, and is significantly important to rocket design. It aids in observing how well a thruster will be able to meet a certain flight mission based on known performance measures. For instance, a small satellite that requires orbit maintenance will need to expend a certain amount of Δv over time; it can be determined if a certain thruster design can achieve this based on analyzing the known performance measures alone. While some performance

measures only apply for certain thermal thruster variants, the ideal rocket equation holds true for all rocket propulsion thrusters and thus has wide application. [11, pp. 100-101]

Electrothermal Thrusters and Resistojets

Electrothermal thrusters are simply rocket propulsion thrusters that operate off electrothermal propulsion. This is defined as propulsion that “comprises all techniques whereby a propellant gas is heated electrically and then expanded through a nozzle to convert its thermal energy to a jet of directed kinetic energy”. [14, p. 90] This idea is quite useful, as it allows for a thruster that still incorporates thermodynamic gas expansion, but without using any processes of combustion. Such an application can provide a high-performance thruster that finds particular use for on-orbit spacecraft. The three most common types of electrothermal thruster include the arcjet, resistojet, and high-frequency excitation, and while all have somewhat different methods for achieving thrust, all operate off the concept of electrothermal propulsion. [14, p. 90] A general conceptual model for a 1-dimensional electrothermal thruster is shown below in Figure 3.

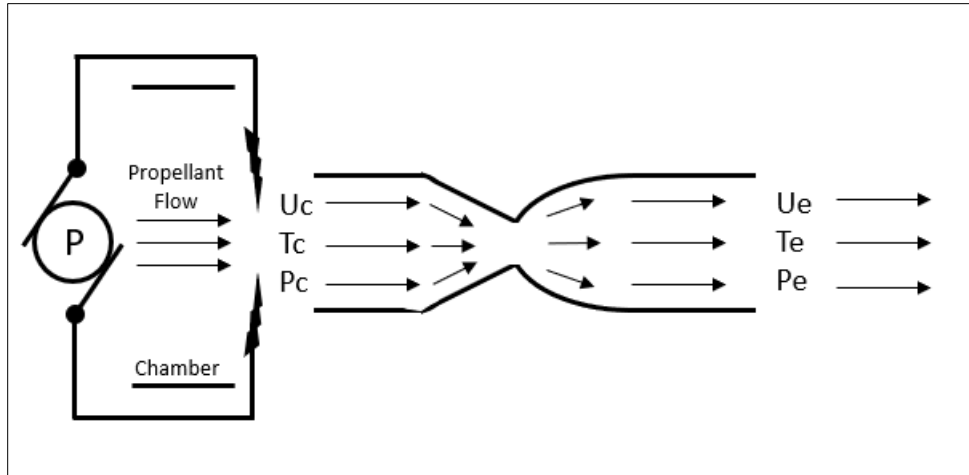


Figure 3. Conceptual Model of Electrothermal Thruster derived from Physics of Electric Propulsion by Robert G. Jahn

As shown, an external supply of electrical power is delivered in some manner, whether it be a solid resistance element, a high current arc, or electrodeless discharge, which then heats a given flow of propellant. This electrically heated gas is then expanded through a supersonic nozzle, giving a high velocity mass flow and usable thrust. Similar to chemical rockets, there is a desire to obtain the highest possible temperature for the propellant flow, as this will give the highest performance. And yet, similar to chemical rockets, there is a limit set by the thermal limitations of the material walls in the prevailing flow. [14]

Alas, while the conceptual model given above holds use for understanding electrothermal thrusters as a concept, it is considered still an ideal model. Real and practical electrothermal thrusters depart considerably from this model in several ways. First, the actual propellant flow is anything but 1-dimensional. Based on the specific

electrical heating mechanism used, vast density and temperature gradients appear in the chamber, and residuals of these gradients can travel into the nozzle and out into the exit exhaust. With these gradients come the viscous and thermal boundary layers that are developed in the flow down the nozzle, with effects manifesting as small nozzle inefficiencies or instead first-order effects that lead to higher performance. [14, p. 92]

Second, a practical electrothermal thruster departs from an ideal model in regards to the radiant heat loss from the thruster body. On a basic level, the electrical input power has some fraction lost to thermal radiation, but this may occur in several ways. The heater mechanism itself may dissipate energy to surrounding thruster elements, which then radiate heat to the environment. The heated propellant flow may radiate heat to the environment itself. The heated propellant flow may conduct heat to the less heated nozzle walls, or the nozzle walls may be heated by viscous dissipation in adjacent boundary layers, and then the nozzle walls radiate to the environment. The heated propellant flow may also have heat radiate out of the nozzle in the axial direction. Since this heat is lost to the environment instead of contributing to the expansion of the propellant flow, there is a reduction in performance compared to the ideal model. [14, pp. 92-93]

While the previously mentioned departures from the ideal model can have sizeable effects, there is a more serious departure. It arises from the “strong temperature dependence of the specific heats of real propellant gases and the inability of these gases to maintain internal energy equilibration during their rapid expansion through the nozzle”. [14, p. 93] This is an issue that can have significant degrading effects on electrothermal thruster performance. Moreover, it means there is heightened importance in the selection of a propellant for a given impulse range. [14, p. 93]

The idea of electrothermal thrusters as a practical application deviating from an ideal model can instead be represented as a collection of efficiencies. The definitions for these efficiencies are given below, taken directly from *Physics of Electric Propulsion* by Robert G. Jahn.

- η_h – “the partial efficiency with which electric energy is delivered from the source to heat the gas stream” [14, p. 93]
- η_a – “the aerodynamic, or nozzle, efficiency with which the stream follows a 1-dimensional adiabatic route through the expansion process” [14, p. 93]
- η_f – “the efficiency with which the thruster converts internal energy in the propellant stream to directed kinetic energy” [14, p. 93]

Using these efficiencies, there can be an accounting for the losses due to the heating process, nozzle viscosity and profile, and unrecovered internal energy in the exhaust jet, respectively. The most latter performance loss is also known as losses due to frozen flow. The overall efficiency of an electrothermal thruster is then the product of these three partial efficiencies, and it is this overall efficiency that is vital in determining the validity of an electrothermal thruster as a useful propulsion system. Even more so, it is the reduction of these losses that is essentially the primary challenge in the development of electrothermal thrusters. [14, p. 93]

Resistojets are considered the simplest type of electrothermal thruster, where the propellant flow is heated by passing over an electrically heated solid surface. The advantage here is that this process can be accomplished several different ways, allowing certain freedom in the actual design. For instance, the heater elements can be constructed

with wire coils aligned parallel to the propellant flow, or instead the chamber walls can be resistively heated themselves; both accomplish the same objective. The main challenges in development of resistojets include overcoming losses due to frozen flow, as discussed previously, heat transfer from the resistance element to the propellant flow, radiation losses from the design as a whole, and the technology of high-temperature materials. [14, p. 103]

Overcoming the challenges of frozen flow losses and achieving effective heat transfer may be approached using analysis with classical heat transfer techniques, but this can become quite difficult based on the geometries and temperature ranges within the thruster. Additionally, substantially varying values for specific heat, thermal conductivity, and gas density through the thruster prevent closed-form solutions. This leads to the eventual finding that analytical solutions of the gas dynamics are not critically important to the application of a resistojet thruster. Instead, experimentation with various propellants, heater design, and chamber design lead rather directly to an acceptable optimization of the bulk flow and geometric parameters for a certain thruster, all without requiring a detailed understanding of the heat transfer model. [14, pp. 103-104]

A similar situation arises when attempting to overcome the challenge of thermal radiation losses. Radiant heat transfer techniques can be used, but in practice using empirical common sense in the design is found to be adequate. For instance, surrounding the active heat transfer duct with insulation or reentrant gas flow passages adequately allows for negligible radiated heat from the thruster body, without the need for analytical heat transfer models. Another design may have the honeycombing of many heater ducts

in parallel, with this array surrounded in insulation, and similarly no analytical model is needed. It should be noted that in the latter design example, such an array is viable from a cost-saving standpoint due to its additional weight being trivial in comparison to the power supply needed to drive the thruster. [14, pp. 104-105]

Still, perhaps the most significant challenge in resistojet development is obtaining high-temperature insulator and conductor materials that can retain electrical integrity and vacuum seals around temperatures of 2500K - 3000 K. For example, tungsten conductors and boron nitride insulators individually hold stable around such temperatures, but when placed in contact form a eutectic compound that is not able to do so. Thermal degradation of the heater element occurs under certain temperatures as well, further threatening the ability of the resistojet to operate. Indeed, the resistojet is most accurately a temperature-limited thruster, and the advancement of high-temperature materials technology could lead to substantial improvements in performance. [14, pp. 105-106]

While not completely intuitive, the simple design choice of the chamber pressure can actually have significant effects on many of the previously discussed challenges that face resistojet development. Selecting a higher chamber pressure reduces losses due to frozen flow by lowering the level of dissociation occurring in the chamber as well as raising recombination rates occurring in the nozzle. This also improves the overall heat transfer from the heater element to the propellant flow, reduces thermal radiation losses through an increase in optical depth of the propellant flow, and allows a smaller chamber and nozzle for a decided mass flow. Still, selecting too high of a chamber pressure brings issues of stress increase on the chamber walls and an increase in nozzle throat erosion,

which can significantly reduce thruster lifetime. The answer then, of course, is a balance between certain pressures, and is historically found to be between 1-5 atm. [14, p. 106]

Although resistojet thrusters do face many challenges in development, the primary goal remains simple: to bring propellant flow temperatures towards the temperature of the surrounding metal. The resistojet can then essentially be thought of as a heat exchanger, and this allows for determination of temperatures along the thruster length using methods of heat transfer analysis. An analysis such as this is considerably simpler if the heater element is presented as heated tubes, which are found in various resistojet designs. Accomplishing this analysis then requires attention of certain flow properties, which are shown below in Equation 37, Equation 38, Equation 39, and Equation 40. [15, pp. 376, 487-488, 507, 514, 520]

$$Re_D = \frac{\rho V D_H}{\mu} = \frac{4\dot{m}}{\pi \mu D_H} \quad (37)$$

where:

$$Re_D = Reynolds\ Number\ [unitless]$$

$$\rho = density \left[\frac{kg}{m^3} \right]$$

$$V = velocity \left[\frac{m}{s} \right]$$

$$D_H = hydraulic\ diameter\ [m]$$

$$\mu = viscosity\ [Pa \cdot s]$$

$$\dot{m} = mass\ flow \left[\frac{kg}{s} \right]$$

$$Nu_D = \frac{h D_H}{k} \approx 0.027 Re_D^{0.8} Pr^{0.4} \quad (turbulent\ flow, Re > 10,000) \quad (38)$$

where:

$$Nu_D = \text{Nusselt Number [unitless]}$$

$$h = \text{film coefficient} \left[\frac{W}{m^2 \cdot K} \right]$$

$$k = \text{thermal conductivity} \left[\frac{W}{m \cdot K} \right]$$

$$Pr = \text{Prandtl Number [unitless]}$$

The equation for Nusselt number has an alternative representation for propellant flows which are considered to be Laminar flow. This is shown below in Equation 39, with the standard definition for Prandtl number shown following in Equation 40.

$$Nu_D = 3.66 \quad (\text{Laminar flow, } Re > 2,300) \quad (39)$$

$$Pr = \frac{\mu C_p}{k} \quad (40)$$

where:

$$Pr = \text{Prandtl Number [unitless]}$$

$$C_p = \text{specific heat at constant pressure} \left[\frac{J}{kg \cdot K} \right]$$

These flow properties are important in the analysis of heat exchangers, as the various relationships between momentum, viscous effects, and thermal diffusion all have an impact on how heat is transferred within the thruster. From here, the found flow properties can be used to obtain the propellant flow temperature as a function of length in the thruster. This is achieved by first analyzing the heat entering the circular tube of propellant flow, where the area term has been modified to fit such a geometry.

$$\dot{q} = hA(T_s - T) = hPdL(T_s - T) \quad (41)$$

where:

\dot{q} = rate of change of heat [W]

h = heat flux coefficient $\left[\frac{W}{m^2 \cdot K} \right]$

P = perimeter of the flow path [m]

dL = some differential length [m]

T_s = surface temperature [K]

T = propellant temperature [K]

Then define the occurring change in temperature.

$$\Delta T = \frac{\dot{q}}{Cp\dot{m}} \quad (42)$$

where:

ΔT = change in temperature [K]

Cp = specific heat at constant pressure $\left[\frac{J}{kg \cdot K} \right]$

\dot{m} = mass flow $\left[\frac{kg}{s} \right]$

Substitute and rearrange:

$$T_0 = T_{in} + \frac{hPdL(T_s - T)}{Cp\dot{m}} \quad (43)$$

where:

T_0 = propellant temperature after heat transfer [K]

T_{in} = propellant temperature before heat transfer [K]

Integrate from $x = 0$ to $x =$ some arbitrary length in the thruster, recognizing that here there is a special heat exchanger condition where the hot fluid heat capacity rate is much greater than the cold fluid heat capacity rate, otherwise known as the condition of a condensing vapor. This condition provides an exponential term for the change in temperature, and can be combined with a log mean temperature difference. This development then arrives at a heat exchanger equation for a resistojet thruster, which is shown below in Equation 44. [15, pp. 8, 676-680]

$$\left[\frac{T_s - T(x)}{T_s - T(0)} \right] = e^{\frac{-P\bar{h}x}{\dot{m}Cp}} \quad (44)$$

where:

$$T_s = \text{surface temperature [K]}$$

$$T(0) = \text{propellant temperature at inlet [K]}$$

$$T(x) = \text{propellant temperature at some length [K]}$$

$$x = \text{arbitrary length in the thruster [m]}$$

$$\bar{h} = \text{heat flux coefficient} \left[\frac{W}{m^2 \cdot K} \right]$$

This analysis allows for determining what the length of the thruster must be if a certain exit temperature is desired, which is an invaluable tool in the initial thruster design.

Overall, the resistojet as a rocket propulsion system has certain challenges it faces in development, but the particular advantages it provides makes it an attractive option for certain missions as an on-orbit thruster. More specifically, it provides thrust levels around 0.5 N, specific impulses around 300 seconds, lower power requirements than other electric thrusters, relatively small impulse bits, and a relatively compact body with low mass. [16, pp. 534, 554]

Tank Design Considerations

Thermal rocket propulsion systems inherently contain pressurized components onboard, as it is the pressurized propellant that leads to a mass flow and usable thrust. Thus, an important design consideration arises with the construction and implementation of the various tanks within a thruster. Before actual design of propellant tanks or refrigerant tanks can be done, it is important to understand the inherent behavior of gases within a tank, as this will drive major design choices. This is best accomplished using the ideal gas law, or equation of state, which is shown below in Equation 45. [17]

$$pV = n\bar{R}T \quad (45)$$

where:

$$p = \text{pressure [Pa]}$$

$$V = \text{volume [m}^3\text{]}$$

$$n = \text{number of moles [moles]}$$

$$\bar{R} = 8.314 \frac{\text{J}}{\text{mol} \cdot \text{K}}$$

$$T = \text{temperature [K]}$$

While the above equation makes use of the universal gas constant \bar{R} , the ideal gas law can also be expressed with a gas constant specific to a certain gas. This is shown below in Equation 46. [17]

$$pV = RT \quad (46)$$

where:

$$R = \text{individual gas constant} \left[\frac{\text{kJ}}{\text{kg} \cdot \text{K}} \right]$$

Understanding the pressure behavior of a gas is vital to tank design, as it allows for analysis of the stress induced on the tank walls. For tanks that can be considered to be shaped as thin-walled cylinders, stress analysis is best accomplished using the concepts of hoop stress and longitudinal stress. These concepts are defined below in Equation 47 and Equation 48. [18]

$$\sigma_z = \frac{pr}{2b} \quad (47)$$

where:

$$\sigma_z = \textit{longitudinal stress [Pa]}$$

$$p = \textit{pressure [Pa]}$$

$$r = \textit{radius of pressure vessel [m]}$$

$$b = \textit{thickness of vessel wall [m]}$$

$$\sigma_\phi = \frac{pr}{b} \quad (48)$$

where:

$$\sigma_\phi = \textit{hoop stress [Pa]}$$

Note how the hoop stress, or circumferential stress, is twice that of the longitudinal stress, or axial stress. This can be used to advantage in designing tanks within thrusters, as eliminating unnecessary wall thickness in a particular direction can reduce the level of inert mass by the thruster, leading to higher performance. [18] In general, the rule of thumb for the aerospace industry is to have a factor of safety between 1.1 and 1.25, and the same applies here in tank design. The chosen material for the tank walls will have a given yield stress, and thus the thickness of the walls should be chosen

so that this yield stress has a factor of safety between 1.1 and 1.25 compared to the stresses induced by the pressurized propellant.

Finally, it is important to look at the pressure behavior of a particular compound that has been used in the past as a propellant, but can also be used as a refrigerant. This compound is known as R-236fa, or hexafluoropropane. The associated vapor pressure dependency plot is shown below in Figure 4.

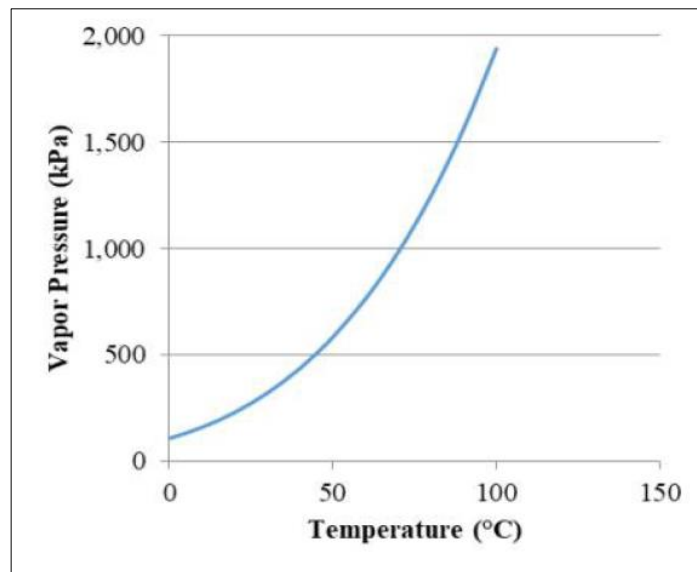


Figure 4. Vapor Pressure Dependency of R-236fa with respect to temperature [19]

Understanding the pressure behavior of R-236fa is important to tank design if using it as a refrigerant, as it will never be expelled from the thruster. This means the tanks used for R-236fa must be designed to handle the pressure behavior of the compound for the entirety of the thruster lifetime.

Small Nozzle Effects

In discussing the heat exchange properties of resistojets, there had been previous discussion on the concept of a Reynolds number, which is the ratio between the momentum and viscous dissipation within a fluid flow. With a high Reynolds number, there is a dominating effect by momentum and properties such as turbulence become more apparent. On the other hand, with a low Reynolds number there is a dominating effect by the viscous forces which results in events such as boundary layers. Observing Equation 37 reveals that Reynolds number is directly proportional to the mass flow of the thruster, and thus there is a follow in logic that smaller thrusters, which produce smaller thrust, and thus have a small mass flow, are considerably more subject to the effects brought upon by lower Reynolds numbers. [19]

From a performance standpoint, one of the more significant effects brought by lower Reynolds numbers is the removal of the isentropic assumption. This is because isentropic flow makes an assumption to neglect viscosity, and at lower Reynolds numbers this does not hold valid. This ultimately leads to a decrease in performance, as typically any deviation from an ideal rocket propulsion system is bound to have such an effect. Specifically, this decrease in performance is manifested as a decrease in the thrust coefficient, or C_F . This decrease in the thrust coefficient leads to less effectively capturing the potential of the characteristic velocity provided by the chamber. [19]

The effects imparted on the thrust coefficient can be traced back to the formation of a boundary layer, an area of reduced velocity that is formed against the thruster walls in the presence of lower Reynolds numbers and is predicted by viscous flow theory. Such effects were quantified by E.W. Spicz with NASA in 1965, using experimental analysis

on small nozzles. This research was then built upon by Christopher Tommila with AFIT in 2017, incorporating more complete analytical methods with generalized compressible flow theory. Tommila arrived at an analytical prediction of the thrust coefficient for lower Reynolds number nozzles based on a given expansion ratio, and the results provided new information that was not quite intuitive. [19]

While higher Reynolds numbers provided the expected increase in thrust coefficient with increasing area ratio, lower Reynolds numbers saw the rapid accumulation of viscous losses with larger area ratios. These viscous losses directly lead to a net loss in thrust coefficient, an outcome not encompassed in ideal models. An important design consideration is then introduced, that small thrusters must be approached differently with regards to the design of the associated nozzle. Small nozzles must be designed with the consideration that a higher area ratio can be detrimental to performance after a certain point. [19]

Small nozzles not only have performance constraints due to lower Reynolds numbers, unfortunately they are also subject to the effects of flow surface roughness due to the microscopically small proportions that are involved. At such nozzle sizes, certain additive manufacturing processes must be used, to include laser powder bed fusion (LPBF). Still, even precise methods such as LPBF leave microscopically small irregularities in the nozzle, manifesting as anomalous protrusions. These protrusions can produce shockwaves within the nozzle that directly impede performance, specifically losses to thrust. This occurs by reflection of the shockwaves off the nozzle walls, which contribute to an overall decrease in the total pressure drop in the nozzle. This pressure drop, in turn, leads to a total loss in thrust coefficient and thrust. Furthermore, the wake

formed behind such irregularities can result in additional drag effects. A topographic figure of a LPBF nozzle generated using a laser scanning microscope is presented below in Figure 5.

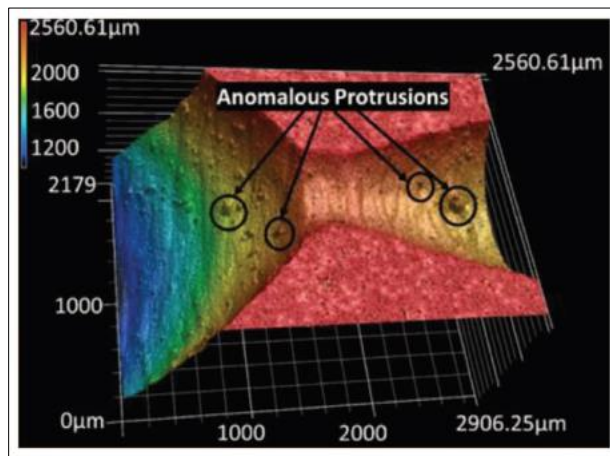


Figure 5. LPBF Nozzle Topography [20]

The anomalous protrusions can be seen here clearly in the figure, and until advanced polishing methods come along, it must be assumed that these losses will be present and thus must be accounted for in expected performance. In general, with current manufacturing technology, small nozzle losses must be planned for in designing smaller rocket propulsion thrusters. [20]

Radiative Heat Transfer Considerations

With electrothermal thrusters such as resistojets operating immensely off the concept of heat transfer, and their typical use as a thruster remaining in on-orbit operation, the significance of the effects brought upon by radiative heat transfer becomes

apparent. Even with the absence of conduction and convection, which is brought upon by operating in the space environment, there still exists several methods by which heat is transferred through radiation alone. Having the general knowledge that all bodies above the temperature of absolute zero radiate heat, there arrives the idea of the overall emissive power coming from a body, which is known as emittance and gives a certain emissivity. Conversely, the well-known Kirchhoff's Law gives a relationship between the emissivity of a body and its corresponding absorptivity, which is the fraction of a total incident energy that is absorbed into the body itself. This concept of absorption is then the first method of radiative heat transfer. This law, developed by Gustav Robert Kirchoff, states that a body which is in thermodynamic equilibrium emits the same level of energy as it absorbs in each wavelength and direction. This law is given below in Equation 49. [21, p. 547]

$$\varepsilon_{\lambda}(T, \theta, \varphi) = \alpha_{\lambda}(T, \theta, \varphi) \quad (49)$$

where:

$$\varepsilon_{\lambda} = \text{emissivity [unitless]}$$

$$\alpha_{\lambda} = \text{absorptivity [unitless]}$$

The remaining methods of radiative heat transfer are then transmittance, which gives a certain transmittivity, and reflectance, which gives a certain reflectivity. The transmittivity of a body is characterized by the fraction of a radiant heat flux that passes through the body, while the reflectivity of a body is then the fraction of a radiant heat flux that is reflected from the body. These methods of absorption, transmittance, and reflectance are then the only methods by which radiative heat transfer can occur, and this is expressed mathematically below in Equation 50. [21, p. 28]

$$1 = \alpha + \rho + \tau \quad (50)$$

where:

$\alpha = \text{absorptivity [unitless]}$

$\rho = \text{reflectivity [unitless]}$

$\tau = \text{transmittivity [unitless]}$

A design consideration is then reached, that perhaps the different radiative heat transfer properties of a certain material can have significant effects on the performance of heat exchangers such as resistojets. While heat may be actively transferring into a desired location, such as propellant, a heat exchanger component with a high emissivity can simultaneously be radiating heat outwards into components that are inhibited by an incident heat flux. A high-temperature material used in such heat exchangers is Inconel 718, which has been studied in its emissivity values. Work done by Keller, Nelson, Walton, Ghosh, Tompson, and Loyalka published in Volume 287 of the journal Nuclear Engineering and Design measured the total hemispherical emissivity for Inconel 718 from roughly 600 K – 1250 K. Results were found for five different surface variations: an “as-received” from the manufacturer, with an air and humidified helium oxidation, with an aluminum oxide powder sandblasting, and with a graphite powder thin coating. These results are shown below in Table 1. [22]

Table 1. Emissivity Values of Inconel 718 [22]

Surface Variation	Temperature Interval	Emissivity
As Received	760 K – 1275 K	0.21 – 0.28
Air Oxidation	650 K – 1200 K	0.2 – 0.52
Humidified Helium Oxidation	600 K – 1200 K	0.2 – 0.35
Aluminum Oxide Powder Sandblasting	780 K – 1270 K 683 K – 1267 K	0.43 – 0.53 (60 grit) 0.45 – 0.57 (120 grit)
Graphite Powder Thin Coating with Previous Sandblasting	650 K – 1200 K	0.60 – 0.70

Similarly, a component within a heat exchanger system that is not the heat exchanger component itself will most likely be made of a different material, and the absorptivity value of this material could lead to undesired heat transfer effects if it is high. Such materials include AlSi12 Aluminum Alloy, which has been studied in its absorptivity values. Work done by Yang, Ying & Gu, Dongdong & Dai, Donghua & ma, and Chenglong in 2018 resulted in absorptivity values calculated for AlSi12 material using ray tracing. Specifically, the laser energy absorption behavior of powder particles was observed using a particular ray tracing method during selective laser melting additive manufacturing of aluminum alloy. The results found that the absorptivity values were sensitive to the sizes of the powder particles. The specific values found for various particle sizes are shown below in Table 2. [23]

Table 2. Absorptivity Values of AlSi12 Aluminum Alloy [23]

Particle Size	Absorptivity
10 μm	0.222
60 μm	0.123

Returning to the idea that all bodies above the temperature of absolute zero emit some flux of radiant energy, or emissive power, there arrives the concept of a black body. In radiative heat transfer, a black body is a theoretical body that is a perfect emitter, and knowing Kirchhoff's Law, also a perfect absorber. Here, all incident radiant energy is absorbed, and thus reflectivity and transmittivity fall to zero. Furthermore, with all radiant energy being perfectly emitted, the dependence of the emissive power of a black body on its temperature can be described with the Stefan-Boltzmann Law, which is shown below in Equation 51.

$$e_b(T) = \sigma T^4 \quad (51)$$

where: $e_b(T) = \text{emissive power} \left[\frac{W}{m^2} \right]$

$T = \text{temperature} [K]$

$$\sigma = 5.670374 \cdot 10^{-8} \left[\frac{W}{m^2 \cdot K^4} \right]$$

This dependence was first established experimentally by Josef Stefan in 1879 and then with thermodynamic argument by Ludwig Boltzmann in 1884. [21, pp. 29-30]

Knowing that radiative heat transfer effects can lead to undesired heat accumulation in a system, an additional design consideration is reached, that perhaps this

can be deterred or at least limited with the application of certain materials. Specifically, this idea has been studied with the implementation of multi-layer insulation (MLI). MLI blankets are a type of thermal insulation that is constructed out of alternating thin sheets of material with high reflectivity. In between these reflective sheets, there is a netted spacer material with low thermal conductivity. This design limits conductive heat transfer, as simply flushing together layers of reflective material would result in conduction and negate any insulation effects. [24]

While the ideal insulation blanket would be a single sheet of reflective material that reflects 100% of incident radiation, this is not quite achievable, thus leading to the multi-layer design. By stacking multiple reflective layers together, higher and higher reflectivity can be achieved. MLI blankets are effective for insulation against thermal radiation, but are considered ineffective for use against conduction or convection. Thus, their use primarily is found in thermal control elements for vacuum applications, most notably spacecraft. MLI blankets can be constructed using a variety of materials; the Habitable Zone Planet Finder (HPF) team at Penn State University uses a combination of 6 μm aluminized Mylar and Tulle for thermal protection of the on-board infrared spectrograph. [24]

Summary

In summary, the fundamentals of general rocket propulsion, concepts of electrothermal thrusters and resistojets, associated methods of heat transfer analysis, various tank design considerations, effects of small nozzles, and different radiative heat transfer considerations are critical and necessary to understand in order to evaluate

different performance values and design effects of a water-propellant resistojet thruster. The understanding of the previously discussed literature will prove vital in the testing environment and bridge the gap between raw data and the accomplishment of the thruster mission objectives.

III. Methodology

Chapter Overview

The purpose of this chapter is to describe the methodology used to characterize the design and performance of the water-propellant resistojet thruster. This includes exploring the interim thruster design in detail, providing details on procedures, equipment, and facilities used in the assembly, integration and experimental testing, outlining the data reduction methods used, examining the methods used to handle data uncertainties, and discussing the expected performance results.

Thruster Design

The resistojet thruster design was an overall compact system (having a total volume of about 1 liter) which would be reliable, minimally hazardous, yet also display high performance. The thruster was designed so that it exhibited certain desirable characteristics, specifically:

- Minimal single-point failures
- Absence of hazardous propellants
- Total volume less than 1 U (10 cm x 10 cm x 10 cm)
- Total mass less than 1.5 kg
- No exotic power requirements

The thermo-electric system used water as the propellant gas and R-236fa as the low-pressure pressurant. The design allowed for the ability of actively controlling feed pressure for throttle control and ensured that neither uncontrolled thrust nor an inability to command thrust could occur if there was an open or closed valve failure. The latter

was made possible by use of four different propellant valves arranged by two parallel sets in series with one another. Additionally, bringing the thruster to life would prove easier than traditional methods as the design primarily held additively manufactured components. AlSi12 Aluminum Alloy was used to print the tank hardware and fluid manifolds, while Inconel 718 was used to print the nozzle and heat exchanger; this ensured an overall ease of manufacturing. While the interim thruster design consisted of these components and other major components discussed below, the assembled thruster design was subject to change due to testing purposes and more. [19]

Pressurant and Propellant Tank

The tank was ring-shaped, had a total internal volume of 271 cm³, with specific dimensions of 60 mm height, 92 mm outside diameter, and 52 mm inside diameter. Separating the pressurant and propellant, there existed a rigid aluminum piston that occupied a minimum volume of 25 cm³. Overall, this allowed a total capacity of 246 cm³, and thus 246 grams, of deionized water as useful propellant. It should be noted that some amount of liquid water, around 1-2 ml, would not be recoverable as useful propellant as it would remain in the propellant feeds positioned between the piston and the valves. The thruster was designed so a pressure greater than 240 kPa (35 psia) could be maintained in the tank at all times, done so by use of R-236fa (having a vapor pressure of 260 kPa, or 38 psia, at 25°C). Overall, the propulsion process needed a minimum of 7.5 grams of R-236fa. It should be noted that while this was the design proposed for actual pressurant use, testing in the laboratory instead used a direct feed line of inert gas. The tank walls had a 1 mm outside diameter thickness and were reinforced with full height bosses for tank lid attachment. Furthermore, the walls had a 2 mm inside diameter thickness and had

shorter mounting bosses for the lid, permitting more insulation space between the heat exchanger and the inside surface of the tank. [19]

Heat Exchanger and Nozzle Assembly

The nozzle design on the resistojet thruster was a conical converging-diverging nozzle with a 20 deg half-angle in the diverging section and an area ratio of 15. The nozzle had a throat diameter of 0.6 mm and was preceded by a convoluted 39-axial-path heat exchanger. This flow path was 2.34 meters long, 2 mm in diameter and was encompassed in the total heat exchanger diameter of 24 mm. The Inconel 718 used in printing allowed for the housing of 4 Watlow Firerod™ heaters and thermocouples, giving temperature control and propellant heating. [19]

Electric Heaters with Integral Thermocouples

The Watlow Firerod™ heaters used in the thruster were 6.35 mm in diameter, 76 mm in length, and generated 15 Watts of heat at an applied 12 V of electrical power. Each heater had an integral Type K thermocouple that was used for heater control. The tank was heated by two of these heaters, while the nozzle and heat exchanger were heated using four. Overall, the heater and thermocouple units provided the ability to heat the propellant gas to improve specific impulse and thrust, the ability to maintain liquid propellant in the tank, and the ability to determine feed pressure on the propellant due to the known tank temperature. The latter was possible by use of the known R-236fa vapor pressure curve. [19]

Pressure Sensor

The pressure sensor used for the R-236fa pressurant was a 19 mm Honeywell pressure sensor. This particular sensor was chosen due to its vacuum compatibility,

compactness, and wide variety of interface packages. The parts selected for this project were 19C200PV4K. Specifications and features included temperature compensation, an upper pressure limit of 1.38 MPa (200 psia), an interface using a 1/8" inch NPT male fitting, and an excitation requirement of 5 Vdc. This higher pressure range allowed for more extensive testing of performance values. [19]

Propellant Control Valves

The valves used to control the propellant flow were The Lee Company IEP Extended Performance Solenoid Valves. Each valve was lightweight and compact, with a mass of about 4.7 grams. The specific model selected was the IEPA1211241H, which was rated to 5.52 MPa (800 psig), provided a temperature range of -20° C to 120° C, and operated on 12 V. As mentioned previously, the resistojet thruster used four valves divided into two parallel pairs, with these pairs arranged in series. This design allowed for the removal of any single point failures, and was a solution for both open and closed valve fails. This is because in the event of a closed valve fail, the parallel valve would simply take the flow, and in the event of an open valve fail, the second pair of valves would prevent an uncontrolled thrust situation. A simple visualization of the thruster valve design is given below in Figure 6. [19]

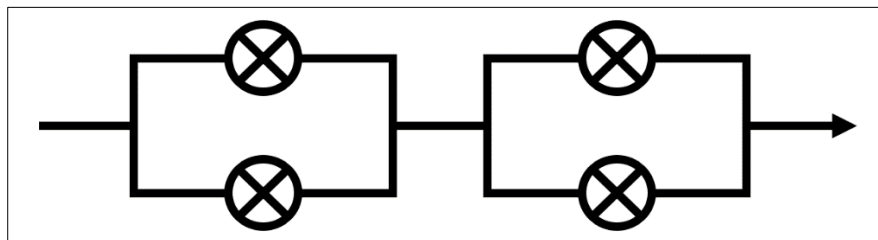


Figure 6. Propellant Control Valve Design

Propellant Metering

Instead of having the propellant control valves determine the mass flow of the system, the interim thruster design had a restrictor put in the flow path to meter the mass flow through the valves. This meter was positioned after the control valve to speed up thruster response. The flow restrictor aperture was quite small, specifically a multi-orifice restrictor with an effective orifice of 0.22 mm. The size of the restrictor would cause an approximate 40 kPa (7 psi) pressure drop when flowing around 54 mg/sec of propellant. This effect, combined with the effects of the exit nozzle throat allowed for a smooth variation in mass flow with pressure change. However, by nature this design choice would also cause shut-down transients to continue longer and produce some loss of effective thrust. The latter was due to the fact that after the closing of the valves, some volume of propellant would be past the valves but before the propellant meter. Instead of being forced through the propellant meter, this residual volume of propellant would boil off, resulting in little contribution to thrust. This effect would additionally result in a reduced system specific impulse, particularly apparent with short and infrequent pulses. Like the propellant control valves, this JEVA series propellant meter was purchased from The Lee Company. [19]

Pressurant System

While a number of pressurant system designs were considered, such as syringe pumps and stepper motor driven pumps, the R-236fa pressurant system was chosen as the final design, as it brought several advantages to the thruster overall. Other designs would require mechanically complex hardware such as gear trains, drive rods, and offset tanks. Along with creating additional points of failure, such hardware would also limit tank

capacity. The R-236fa pressure system operated simply off temperature control, which was a required capability for the thruster regardless, as the propellant was not allowed to freeze in order to maintain proper thruster operation. This design gave maximum tank size and improved reliability with the absence of moving parts. Hexafluoropropane (R-236fa) was the specific compound chosen for the pressurant due to its significant increases to pressure in response to fairly small temperature changes. The curve for vapor pressure dependency to temperature for R-236fa is given in Figure 4, which is found in Chapter 2. [19]

System Layout

Figure 7 shows a Computer Aided Design (CAD) of the thruster system external layout as well as an angled cut plane through the thruster. From the figure, the layout of the previously discussed system components can be identified. Four Watlow Firerod™ heater units are placed surrounding the heat exchanger and nozzle assembly, and two heater units are placed near the pressurant tank and propellant tank. The pressurant pressure sensor and the pressurant fill valve are placed on the top of the thruster, while the propellant valves run vertically along the front. The propellant fill port is placed on the outside of the tank, and is shown in Figure 7 as closed with a pipe plug at the top. [19]

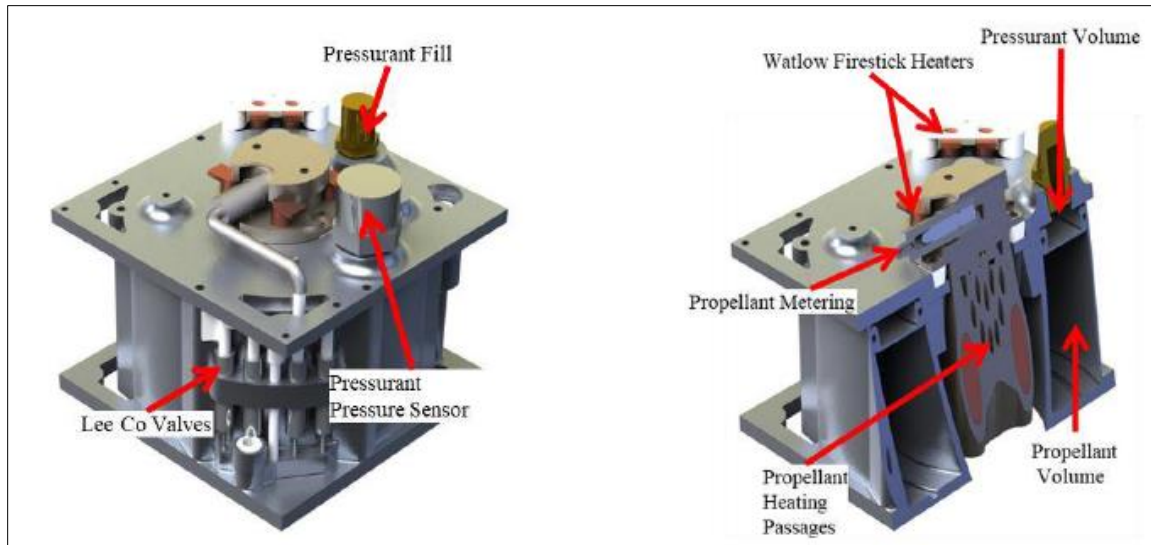


Figure 7. Computer Aided Design of Thruster System Layout [19]

Assembly and Integration

Before testing of the thruster could begin, a rather obvious step needed was the assembly of the thruster and its integration into the testing bed. Given the thruster was designed for use as an on-orbit system, testing needed to be performed within a vacuum chamber. Following, use of one of the vacuum chamber facilities at AFIT became routine. Pictured below in Figure 8 is the facility that was used during the assembly, integration, and testing period; it is known as the Geo-orbital Nano-thrusters Analysis and Testing Laboratory (GNAT).

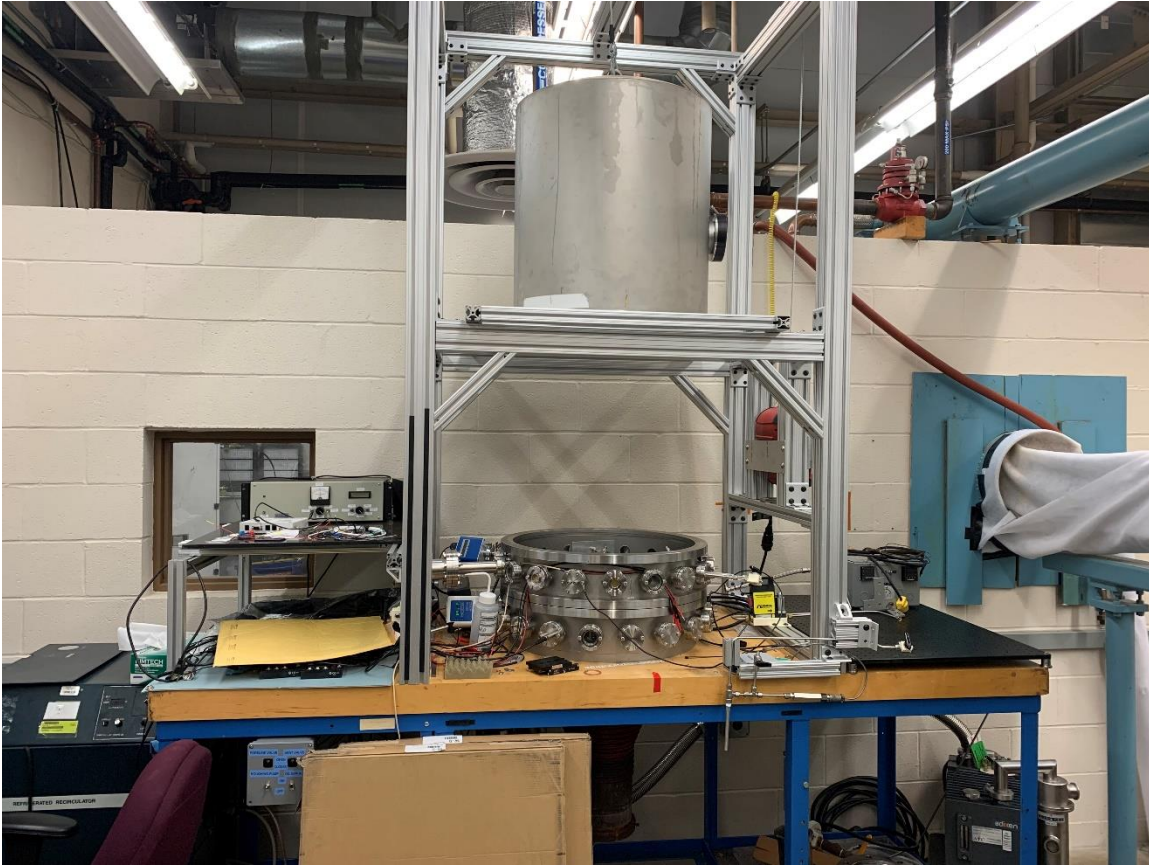


Figure 8. Initial Setup of Vacuum Chamber Facility

Due to the vacuum chamber being in use by other research projects as well, some modifications had to be made in order to accomplish the testing objectives. Three different flanges had to be installed onto the chamber to allow for testing: a thermocouple passthrough flange for taking temperature measurements, a canon plug flange for signals and power, and a load cell flange for data acquisition. Pictured below in Figure 9 and Figure 10 are the first two of these flanges.

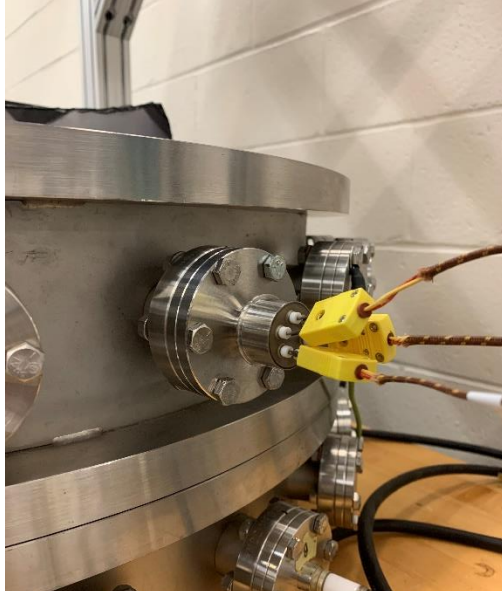


Figure 9. Thermocouple Flange



Figure 10. Canon Plug Flange

While the thermocouple passthrough flange was rather simple to install, requiring just the attachment of thermocouple wire extensions onto the exterior of the flange, the canon plug flange had to be custom adapted for the needs of the testing. Various wiring for the pressure sensor, heaters, propellant control valves, and load cells (strain gauges) had to be individually assigned and implanted into different pins, a process that was rather tedious. This wiring harness was made for both external connections and internal connections, with the canon plug flange being the point of attachment. A full view of the external wiring harness that was constructed for the vacuum chamber is shown below in Figure 11; the internal wiring harness was quite similar except for its absence of spiral wrap as to not contribute to chamber contamination.



Figure 11. External Wiring Harness

The load cell flange was also rather simple to install, as the accompanying wiring harness had already been assembled previously for use in past research. Installation then became a simple task of connecting the harness to the external electrical port of the flange.



Figure 12. Load Cell Flange

Moving forward, it was decided that in the interest of improving instrument organization for the current research as well as future research conducted in the GNAT laboratory, an instrument bed should be constructed near the vacuum chamber. Proceeding, a series of terminal boards were then installed into the side of the instrument bed, where they could be interfaced with the external wiring harness. This process involved wire stripping and terminal crimping for every individual wire, and then assigning and fastening each wire to a selected terminal port. Even still, the installation of the terminal boards required the design and construction of a 3D printed adapter to allow for proper fastening on to the instrument bed. Pictured below is the initial build for the instrument bed, the 3D printed adapter, and the terminal board interface.

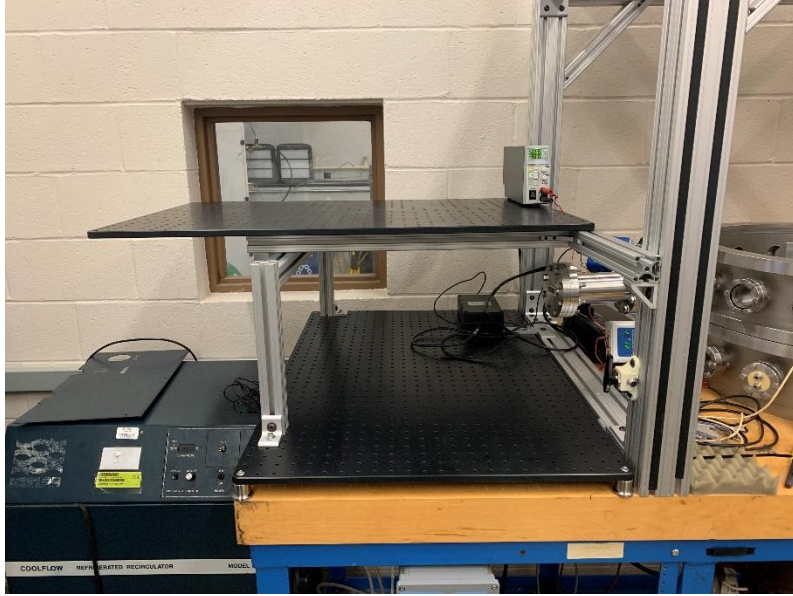


Figure 13. Initial Build of Instrument Bed

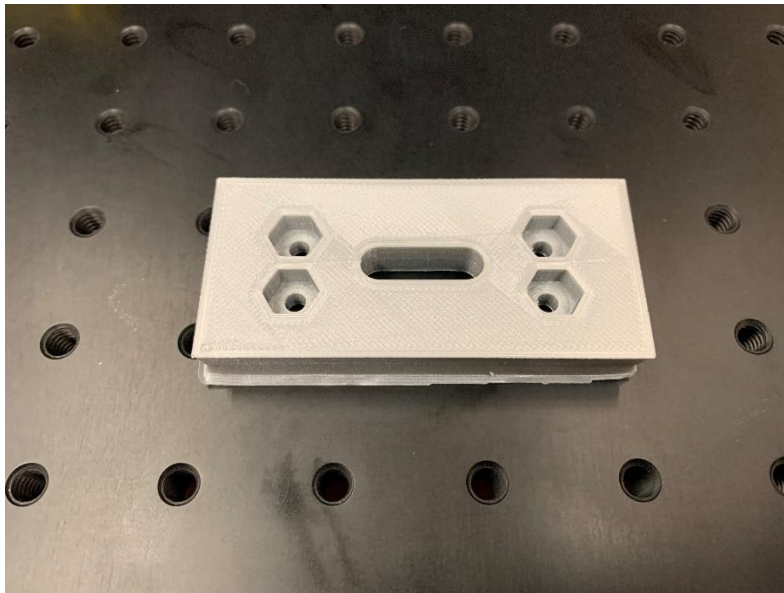


Figure 14. 3D Printed Adapter

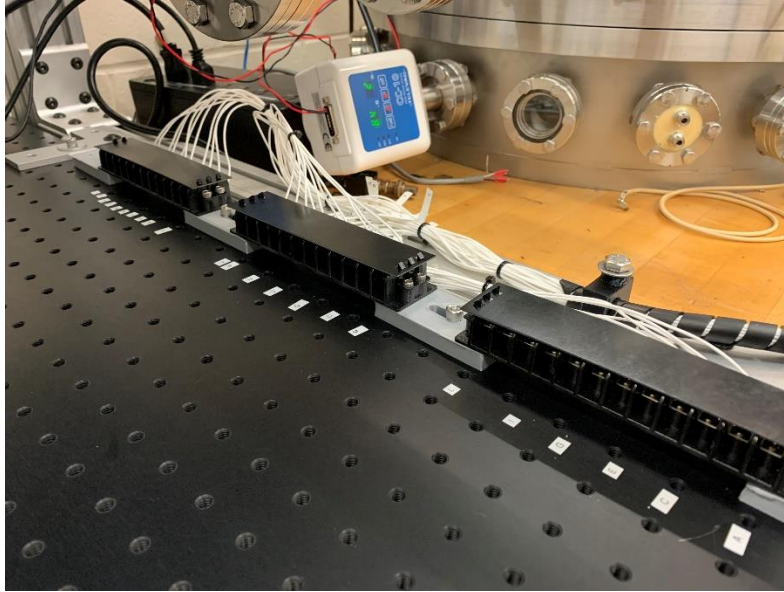


Figure 15. External Terminal Board Interface

In a similar fashion, the existing test bed structure for the thrust stand within the vacuum chamber was modified with the installation of terminal boards as well. This also required design and construction of various 3D printed adapters to allow for proper fastening to the test bed structure. These adapters were similar in application to the adapters used outside the chamber, but with slightly different designs. Furthermore, a graphite sheet was installed underneath the test bed structure to mitigate contamination by residual oil within the chamber. The present oil was a result of the vacuum chamber being operated with an oil diffusion vacuum pump. Proceeding, the internal wiring harness was then interfaced with the terminal boards, leading to a similar setup as seen outside the chamber. This internal terminal board interface with the accompanying underlying graphite sheet is pictured below in Figure 16.

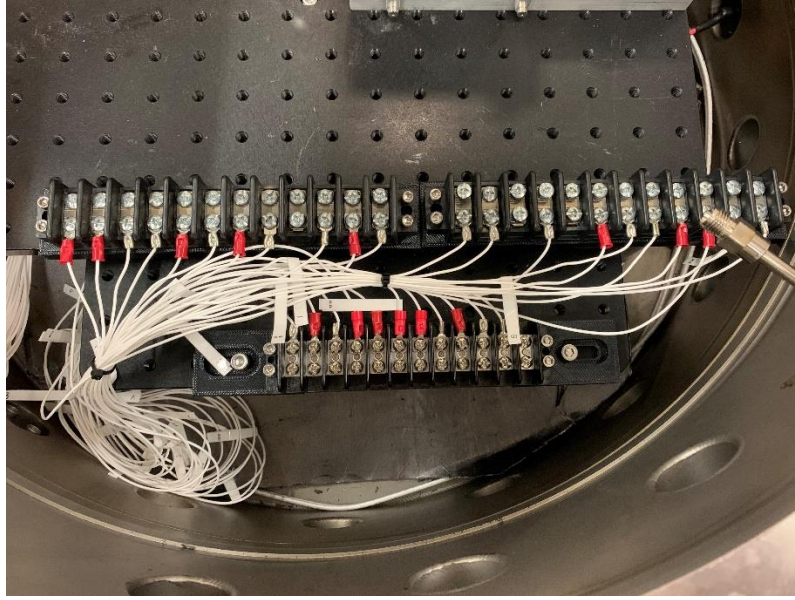


Figure 16. Internal Terminal Board Interface

With a good portion of the electrical setup complete, attention was shifted to the primary testing instrument, the thrust stand. Used previously in past research, the design of the thrust stand followed that of an inverted pendulum, where the thruster would sit atop a platform attached to 4 vertical arms and push against a strain gauge as thrust was applied. The applied force against this strain gauge would then be measured and sent out as data through the wiring harnesses. However, the thruster being tested in this research had never been tested on this thrust stand, and thus an adapter was needed in order to have a proper fit. As done previously with the other adapters, this new adapter was designed using CAD and then constructed using 3D printing. Still, while the new adapter was assumed to have been designed correctly, actually fitting the thruster onto the adapter revealed some misalignment issues. Thus, a Dremel[®] tool was then introduced against certain areas of the adapter, and after some coordinated material removal the thruster was

then able to fit properly. Pictured below is the adapter used to interface the thruster with the thrust stand, after having been adjusted by the Dremel[®] tool.



Figure 17. Adjusted Thrust Stand Adapter

All while the vacuum chamber was being modified to fit the testing objectives, simultaneously the resistojet thruster was undergoing assembly and receiving modifications of its own. Larger pieces such as the main thruster body, the top interface, and the heater block were additively manufactured and smaller pieces such as the heaters and the propellant control valves were already fully constructed, leading to the execution of putting together the thruster becoming truly a simple assembly instead of a complex construction. Still, fitting the pieces together required some various adjustments, with the first appearing as a modification of the propellant control valves. In order to install the valves into the flow path, the tubes leading in and out of the valves had to be the proper length so to fit correctly onto the side of the main thruster body. As the valve given tube

lengths were longer than desired, various tube shortening was required. This was done simply by use of a 1/16 inch tube cutter.

Even with the control valve interface on the side of the main thruster body being specifically designed to fit the control valves, inconsistencies in the additive manufacturing led to the need for adjustment drilling. Once completed, the propellant control valves fit snugly into place within the interface, and permanent installation could begin. This installation involved the application of epoxy to areas of the thruster where separate pieces joined together, including the addition of the additively-manufactured control valve manifold which connected the control valves within the flow path; this epoxy provided a seal to ensure the integrity of the flow path. Additionally, the outdated propellant meter interface that was implemented into the thruster design was shortened by a Dremel[®] tool and plugged using epoxy and a spare screw; this allowed the propellant control valves to fit into the interface and also ensured the integrity of the flow path. Finally, the electrical leads of the propellant control valves were soldered into outgoing wires, where they would eventually be connected to an external power supply when testing began. The resulting adjustments to the thruster are showcased below in Figure 18.

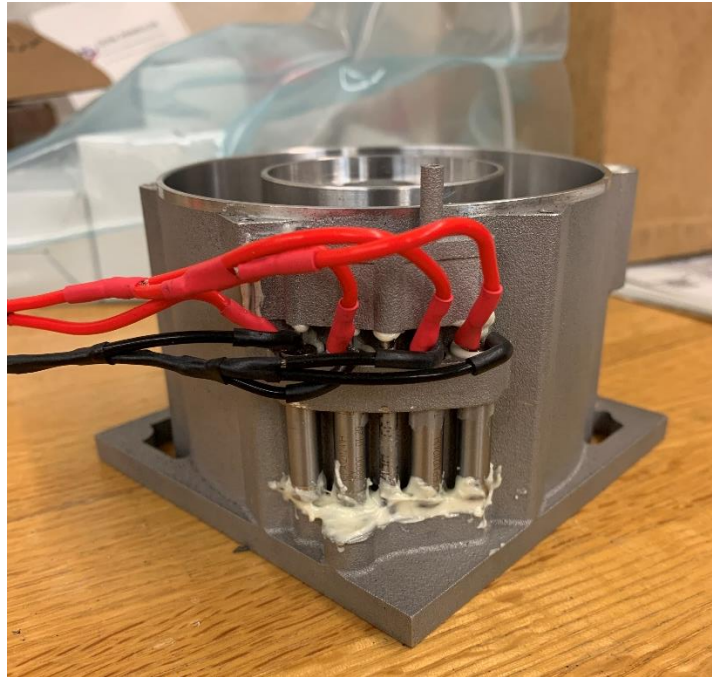


Figure 18. Thruster Adjustments

Having the necessary adjustments made to the thruster, some verification was needed that these adjustments allowed for proper function of the flow path. To do this, a simple check was performed that propellant would flow out of the tank into the valves, and also that propellant would flow out of the valves. This was accomplished by assembling the tank piston, filling the propellant tank with de-ionized water, and manually pressing down on the piston into the propellant tank. The check exhibited de-ionized water successfully exiting the propellant control valves, verifying the integrity of the flow path. This check also revealed proper function of the propellant control valves and the seal integrity of the piston, as when the control valves were closed there was a pushback of force against pressing down on the piston. Shortly after, an adapter piece

was reshaped using a belt sander and attached to the exit of the propellant control valves, which was then topped with a tube union that would allow for a flow path from the propellant control valves to the entrance of the heater block. Following the attachment of this tube union, an additional flow check was performed, and resulted as previously.

With these steps completed, the process of mounting the top plate of the thruster could begin. Due to this plate mounting signifying the arrival of the final steps in the thruster assembly, the propellant tank was filled with de-ionized water for the final time, and the tank piston was fully assembled and installed, sealing the propellant inside for use for when the thruster would be fired. After successfully installing the piston deep enough into the tank, the top plate was mounted on to the thruster and screwed down. With the top plate mounted, the heater block could be installed into the thruster and integrated into the flow path. To do this, ceramic risers were first inserted encompassing the screws mounting the heater block to the thruster. This was implemented to physically raise the wider top of the heater block away from the surrounding aluminum of the thruster body, as there existed the possibility of the aluminum melting if in close enough proximity to the heater block. With the risers placed, the heater block was then screwed down into the thruster.

Following the installation of the previously mentioned pieces, the vast majority of the thruster had been assembled and only some final touches remained. Both the pressurant fill port and the pressurant pressure sensor were screwed into their respective ports using Teflon tape to ensure a proper seal. The final piece of the flow path was then the 1/16" tube connecting the propellant control valves to the entrance of the heater block. While the heater block itself only required the attachment of an adapter that

allowed for tube connection, the 1/16" tube itself required some modification. To properly flow into the heater block, the tube was bent into various turns; this was done using a 1/16" tube bender. After the attachment of this tube, the heaters were simply inserted into their respective ports, and thus the final piece of the resistojet had been installed and the thruster was assumed complete.

However, a verification test needed to be performed on the pressurant volume to validate that proper seals were being maintained. Thus, the pressurant volume was filled with 100 psi of inert gas, and resulted in an almost immediate expulsion of water out of the propellant control valves. This posed an issue, as the pressurant verification test inadvertently revealed a previously unknown malfunction in the control valves. After some inspection and outside research, the malfunction was found to originate from an improper installation within the flow path. As most control valves do not have a defined inlet and outlet, this was not something that was taken into consideration when installing. Since The Lee Company valves were designed with a certain architecture that gave a defined inlet and outlet, it resulted in the installation of the valves in an accidental flipped orientation. Furthermore, since these control valves were applied to the thruster using epoxy, the only way forward was to perform future tests with these valves constantly open, and instead attach a new, properly installed valve ahead of the original control valves in the flow path.

With the propellant flow path fixed, the original purpose of validating the proper seal of the pressurant volume could be accomplished. Once again, the pressurant volume was filled with 100 psi of inert gas, but now resulted in an almost immediate depressurization. This also posed an issue, as the test showed that the pressurant volume

was in fact not sealed. After some inspection, it was suspected that one of the O-rings was not providing a proper seal. Thus, a new size O-ring was installed and room temperature vulcanizing silicone (RTV) was applied to ensure a seal. An additional pressure check was performed, and this led to a depressurization as well; although this was noticeably less rapid. More inspection was performed, and it was discovered that along with the pressurant leak coming out of the pressure sensor and pressurant fill port interfaces, propellant was leaking out the manifold connecting the original control valves together. To solve these issues, epoxy was completely applied over the entire volume of the control valves, and RTV was applied into the thread of the two top plate interfaces.

After allowing the epoxy and RTV to dry, a pressurant pressure check was performed once more. Unlike the other tests, this new test resulted in a somewhat stable, sealed pressurant volume that decently held 100 psi. Still, while the new leak rate was noticeably slower, it was still measurable over a period of time. This leak rate remained under 1 psi/min and drifted towards an even slower leak rate over time. This rate was deemed sufficient for the purposes of testing, as this removed the need for a roughing pump for the vacuum chamber, and the pressurant volume would still be held at a constant pressure by an external tank regardless. With the pressurant volume being validated, the next step of verifying thruster function could begin.

While epoxy had been applied previously to fix a propellant leak out of the propellant control valves, this had been done only when performing a pressurant volume integrity check. Verification was needed that with the propellant control valves open and propellant actively flowing, there would still be an absence of propellant leaks. Thus, the thruster was pressurized and the propellant control valves were opened, and this led to a

noticeable leak of propellant. As done before, epoxy was applied to the leak source and allowed to harden. This process was repeated for several leaks, as one leak would emerge when another leak was resolved.

After many attempts to fully seal all possible leaks, eventually a leak check was performed that showed a leak determined to be miniscule enough for testing purposes. While this continuous loss of propellant meant that the specific impulse would not be measurable for the thruster, the thrust still would be. With the thruster unable to be realized as fully functional, testing procedure moved to measuring thrust alone, as this performance measure was independent of propellant loss. Thus, for the second time, the thruster was assumed complete and ready for testing. Figure 19 below shows the completed design for the water-propellant resistojet thruster that would be used in testing, seen here atop the thrust stand and thrust stand adapter.

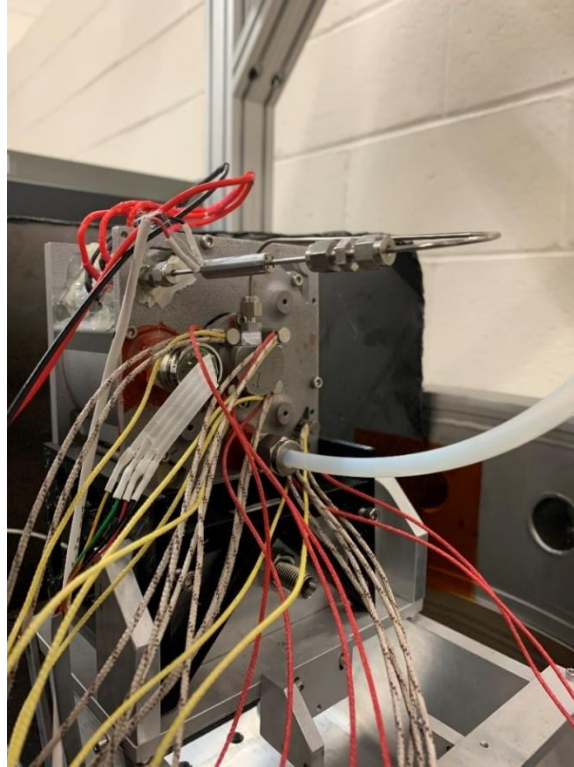


Figure 19. Water-Propellant Resistojet Thruster

With the previous functional testing of the thruster requiring an electrical connection between the propellant control valve system and an external power supply, as well as a gas connection between the pressurant volume and an external pressurant tank, completion of the remaining wiring and instrument setup was begun. Wiring from the pressurant pressure sensor, heaters, and propellant control valve system was wired to the internal terminal board. The load cell had an individual, designated connection with a wiring harness that led out of an isolated flange, and thus was not wired to the internal terminal board. Additionally, a pressure sensor that would be used for future work in the GNAT laboratory was wired to the internal terminal board. These connections are shown below in Figure 20.

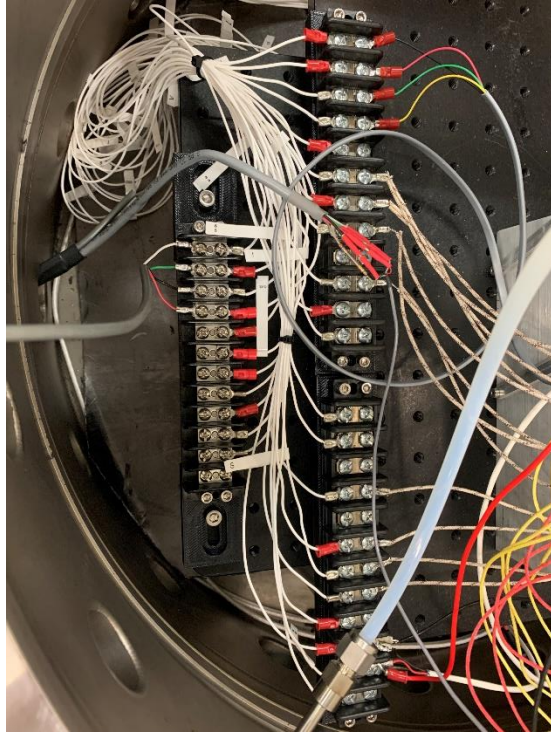


Figure 20. Wired Internal Instrument Board

The thermocouple units within the heaters were then wired to the thermocouple flange connection, which would allow for heater temperature control when testing began.

Additionally, a gas connection was made between the pressurant fill port and an existing flange port that led to an external pressurant tank. With this, the internal wiring for the vacuum chamber was complete. These connections are shown below in Figure 21.

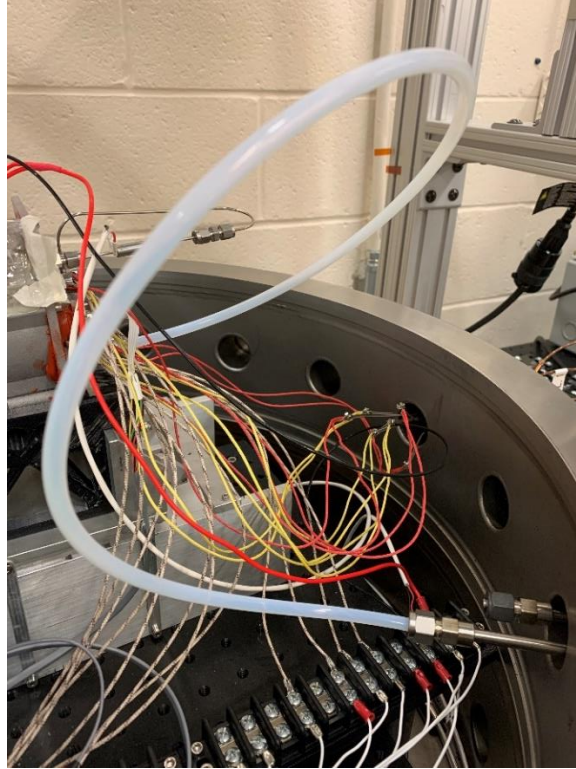


Figure 21. Thermocouple Wiring and Pressurant Hookup

With the various modifications being made to the vacuum chamber and the thruster, the point had arrived of setting up the external instruments that would be needed for testing. The previously constructed instrument bed was then put to use, holding the different instruments needed to power and interface with the heaters, controllers, propellant control valves, load cells, and sensors. Additionally, a simple flat structure was mounted to fit in the controllers, which were subsequently secured down. In total, three controllers were used to control the six heaters, which were broken up into one controller assigned to the propellant tank heaters and two controllers assigned to two respective heater block heaters, labeled Heater Block 1 and Heater Block 2. This controller setup and accompanying mount are shown below in Figure 22.

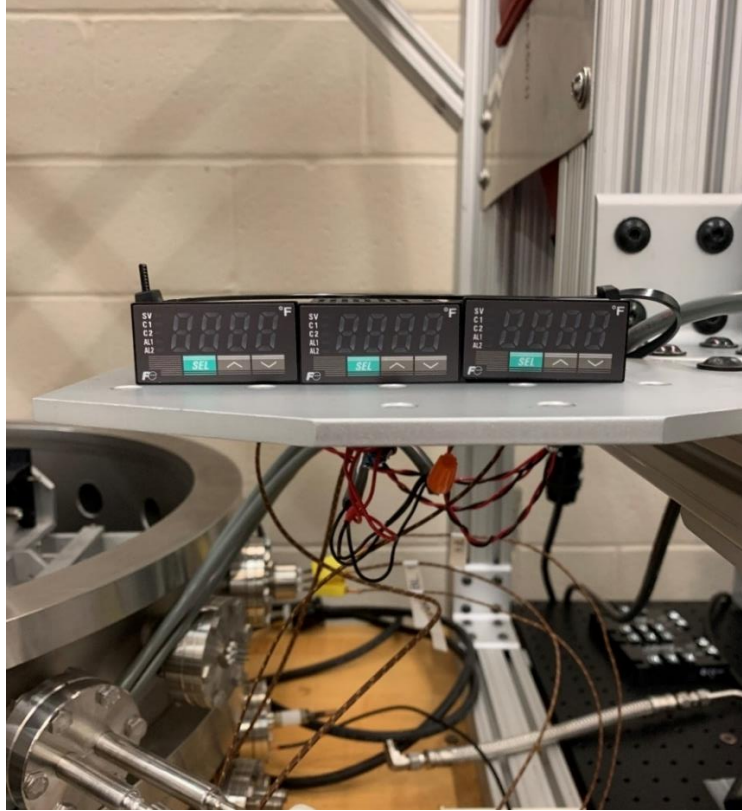


Figure 22. Controller Setup

The relay ports of the controllers were then electrically connected to the terminal board assignments of the heaters, followed by the controllers being connected to the needed power supply and the thermocouples, leaving only the connection of the heaters themselves as the final missing piece of the controller circuit, which had been placed with thruster integration. However, to improve wiring organization and overall safety, a switch box was integrated into the controller circuit as well. While the controllers themselves had internal switches, the decision was made to incorporate a separated switch when splitting the power cable to the controllers. This switch setup is pictured below in Figure 23 and Figure 24.



Figure 23. Switch Box Interior



Figure 24. Switch Box Setup

Appropriate wiring was then fed out of the external terminal board and connected to the proper external instruments. The heaters and propellant control valve system were wired exclusively to various power supplies, while the pressure sensor and load cell were wired to a data acquisition board, which would take pressurant pressure data and force data when testing began. A vacuum pressure sensor that had been previously installed onto the chamber was also wired to the data acquisition board. This board was then wired to a designated computer that would process the future data through LabView. Finally, the outgoing gas connection flange on the vacuum chamber was connected to an external tank, which would provide the pressurant when testing began. This setup is pictured below in Figure 25, Figure 26, Figure 27, Figure 28, Figure 29, and Figure 30.

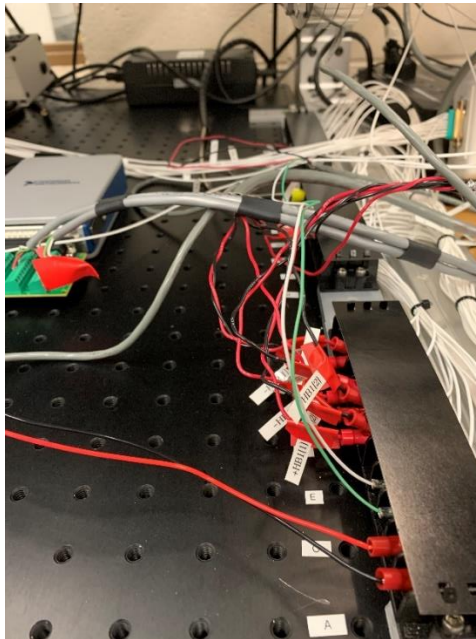


Figure 25. External Wiring



Figure 26. External Power Supplies

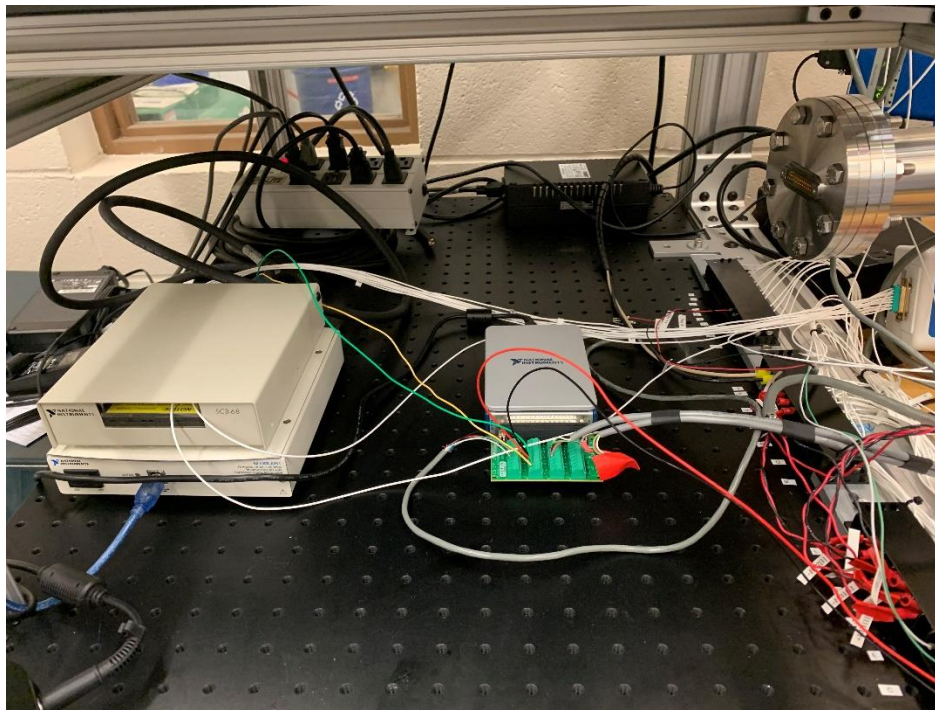


Figure 27. Data Acquisition Board Setup

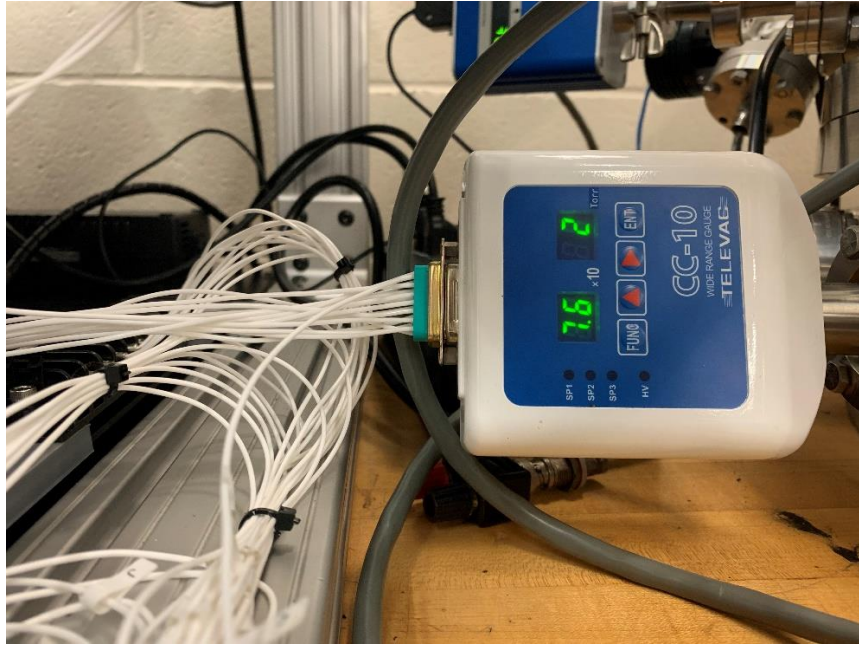


Figure 28. Vacuum Chamber Sensor

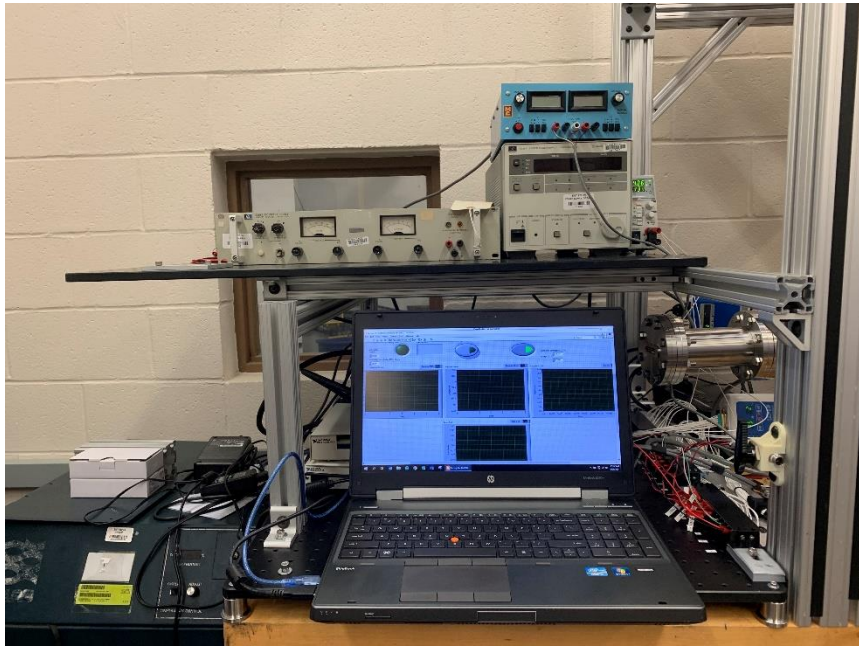


Figure 29. External Instrument Setup



Figure 30. External Gas Tank Setup

With the vast majority of the wiring having been set up, a functional check of the heaters was performed to observe that proper temperatures would be reached and that the different heater pairs would be controllable. As power was provided to the heaters, they began to slowly rise in temperature until around 160 °F when smoke was seen rising from the micro-controllers. The conclusion was reached that somehow a higher current was being provided to the controllers than what they were rated for, which was around 3 amps. To overcome this problem, an additional set of relays was introduced into the controller circuit. With this new addition, a functional check of the heaters no longer showed a damaging current flowing through the controllers. These new relays integrated into the controller circuit are shown below in Figure 31.



Figure 31. Additional Relay Set

However, while the absence of smoke allowed for the heater temperatures to rise higher, it revealed that the controllers were not able to control the heaters to the desired temperature, and instead the temperatures were rising uncontrollably. After some inspection, it was concluded that the controllers were delivering only roughly 20 milliAmps, yet the new additional relays required around 140 milliAmps to activate. This disparity led to the inability to control the heater temperatures, and thus a new set of relays were needed for the controller circuit. Specifically, the proposed solution was the implementation of solid-state relays, which operated off a much lower activation current. With this addition, a new functional check of the heaters was performed, and once more displayed an inability to effectively control the heaters to a desired temperature. After

even more inspection, it was concluded that these new relays were ineffective due to a rather high resistance occurring across the switch component of the relay. Thus, the decision was made to perform future testing in this uncontrolled state, as the capability to control to an exact temperature was not immediate and necessary as was the capability to generally raise the heaters to high temperatures, which had already been demonstrated.

Due to the sensitivity and fragileness of the sensor, the load cell was purposefully designated as the last remaining piece of the test bed. Thus, a thruster functional check was required beforehand as to ensure a smooth transition into testing and no complications once the vacuum chamber was sealed. The heaters were warmed to an appropriate temperature, the pressurant volume was pressurized to 40 psi, and the propellant control valves were then opened, allowing for propellant to flow through the thruster. After several seconds of observation, it was found that the previous leak assumed to be minuscule enough for testing was in fact not miniscule at all. The present leak prevented propellant from properly flowing through the thruster, and resulted in the inability of the thruster to produce any thrust. With this, the water-propellant resistojet thruster failed the required functional check to enter performance testing, and thus testing procedure moved on to evaluation of design effects.

Experimental Testing

With the controller, heater, and wiring setup fully assembled, experimental testing of the heat losses coming from the resistor component of the thruster became quite straightforward. Due to the solid-state relays remaining unable to control the heater temperatures, all relays were disconnected from the heater circuit and power was fed

straight into the heaters. With the thermocouple connections remaining as the only connected controller wiring, the controllers became simple temperature readers, and would remain as the primary method for temperature data collection. Due to the scope of this experiment focusing on the effects of resistor heat loss on the thruster propellant tank, the final circuit check designated the temperature readings of Heater Block 1, Heater Block 2, and Tank as active, the supplied power to Heater Block 1 and Heater Block 2 as active, and the supplied power to Tank as inactive. With this, setup for experimental testing was complete and testing procedure could begin. Pictured below in Figure 32 is the described temperature reading setup, with all relays disconnected.



Figure 32. Temperature Reading Setup

The experiment was first performed with the vacuum chamber open, mainly to act as a practice run before sealing the vacuum chamber, but also for the added benefit of

observing how the added component of convective heat transfer affected the results. The heater power supply was turned on, and set to provide a power level of roughly 53 W. Slowly over time, the temperatures of the heater block would rise, and the temperature of the propellant tank would rise as well. Temperature readings were recorded every 1 minute in the initial readings, and recorded every 4 minutes in the later readings. This data was collected for roughly 90 minutes, a collection period chosen purposefully to reflect the orbital period of satellites in low Earth orbit.

After the data collection period was finished, the heater power supply was turned off and the thruster allowed to cool off. The same procedure was repeated, but now with the vacuum chamber sealed and the chamber pump turned on to create a near-vacuum environment of 7.7×10^{-2} torr. During this data collection period, it was discovered that the temperature readouts malfunction as the temperature approaches 800° F, and thus the set power level was reduced to a much lower value compared to the power level used with the open chamber, specifically 20.6 W. This allowed for an eventual near-steady-state condition for the heaters, with the power balance being reached between the input power and the outward-radiated power resulting in a near-constant heater temperature. Figure 33 and Figure 34 below depict the experiment setup with the sealed vacuum chamber and the resistojet thruster mounted inside the chamber during testing.

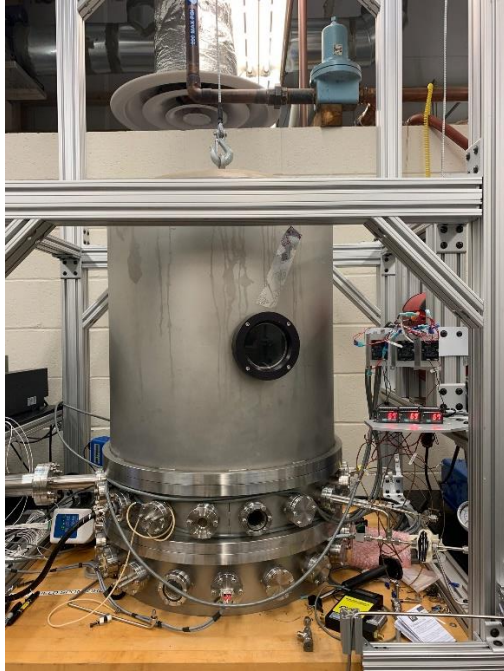


Figure 33. Heat Loss Experiment Setup



Figure 34. Thruster in Testing

With the previously mentioned propellant leak preventing the resistojet from producing any meaningful thrust, performance testing was ruled unachievable. Yet, this did not mean that functional testing of the heater block itself was unachievable; if the propellant tank and control valve system were completely bypassed and propellant was fed directly into the heater block, this would allow for a functional check of the heater block to verify that propellant was properly flowing, high-temperature steam was being achieved, and a general propulsive force was being produced. Thus, the gas connection used previously to provide pressurant to the pressurant volume was repurposed; de-ionized water was filled into the gas connection and cleared of most air pockets. Following, one end of the gas connection was connected to the inert gas tank while the other connection was connected directly into the heater block, bypassing all systems. Thereby, release of inert gas regulated to 40 psi would force propellant through the heater block and produce an observable thrust. The direct connection made between this gas connection and the heater block is shown below in Figure 35.

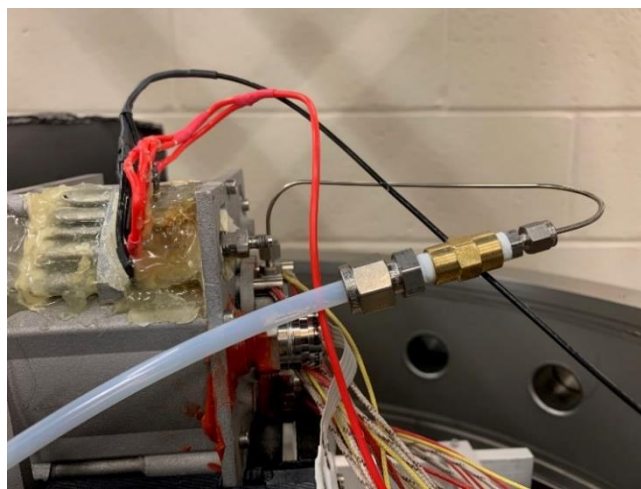


Figure 35. Tank and Valve System Bypass

After the completion of the direct connection, the resulting test procedures simply consisted of releasing the inert gas and visually observing the results, verifying that the heater block functioned as intended.

Data Reduction

While the raw data recorded in the heat loss experimental testing consisted of just three fluctuating temperatures and was thus rather simple, it should be noted that the two heater block temperature readouts were measuring the temperature of the same component. Following, the difference in temperatures recorded by Heater Block 1 and Heater Block 2 was more so a disagreement between the thermocouples of the various heater rods, and the actual temperature of the heater block overall was some temperature in between, perhaps the average. Thus, for the purposes of data reduction, the average temperature between Heater Block 1 and Heater Block 2 was calculated for each data sample and taken as the accepted value for the overall temperature of the heater block.

Data Uncertainty and Experimental Error

As mentioned previously, it was discovered that as the temperature of a heater approached 800° F, the temperature readout would begin to malfunction. Specifically, this malfunction ceased the display of a listed temperature, and thus resulted in the exclusion of a known data point in the overall sample. To overcome this data uncertainty, simple interpolation was used where necessary. Additionally, the discovery of the temperature readout malfunction resulted in unplanned alterations to the heater input power mid-experiment in the attempt to lower the heater temperatures away from 800° F. This resulted in fluctuations of the heater block temperatures not seen in the temperature

data of the open chamber experiment, where the malfunction went undetected. No action was taken to address these data fluctuations, as they did not change the heat loss effects felt by the thruster propellant tank and thus was not necessary to resolve. Still, it explains the erratic heater block temperatures seen in the temperature data of the closed chamber experiment.

Expected Performance Results

In a paper written for the AIAA SciTech 2021 Forum, members Hartsfield, Shelton, and Cobb presented the expected performance of this thruster design for thrust and specific impulse, as well as additional impacts. It was predicted that due to the effects of small nozzles such as low Reynolds numbers and anomalous protrusions, the expected thrust coefficient for the thruster would be much lower compared to the isentropic estimate. Data from previous work was taken, specifically work done by Chris Tommila, and an assessment was made that the thrust coefficient would have an expected value of approximately 1.0. Using this prediction, the expected tank pressure (derived from tank temperature and the known behavior of hexafluoropropane), the expected pressure drops across the metering orifice, and the heating passages in the nozzle and heater block, a derivation of the resistojet thruster expected thrust behavior could be made. This derived expected thrust behavior is shown below in Figure 36.

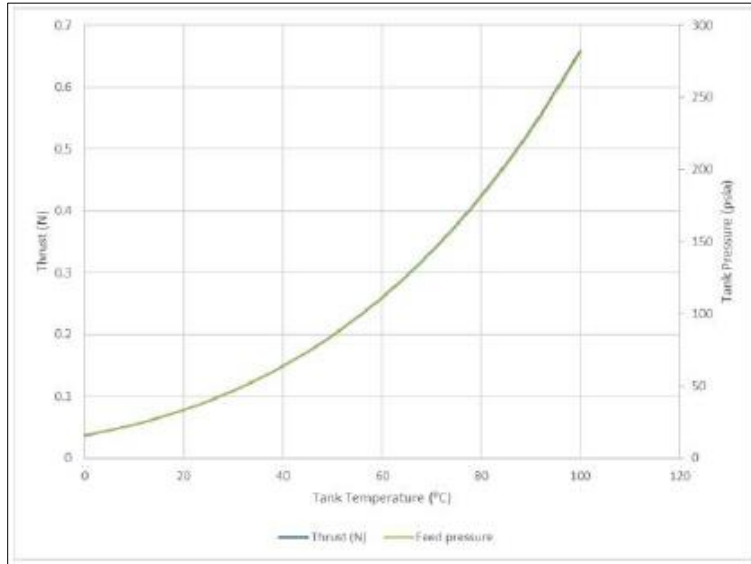


Figure 36. Expected Thrust Performance of Resistojet Thruster [19]

From the data, it is expected that at the nominal operating conditions of 30°-50° C in the propellant tank, there will be thrust levels around 0.1 N – 0.2 N. Still, it is shown that these thrust levels could triple with a tank temperature increase to 100° C. [19]

A comprehensive prediction of the specific impulse performance was also made for the resistojet thruster. The expected specific impulse performance for the thruster was found to be primarily a function of the heater block temperature. Due to the effective design of the heater passage, it was predicted that by the time it reaches the nozzle entrance, the propellant gas would be very nearly the same temperature as the metal in the heater block. Using various thermodynamic relationships, the expected trend then became a square root of the absolute temperature. This derived expected specific impulse behavior for the resistojet thruster is shown below in Figure 37.

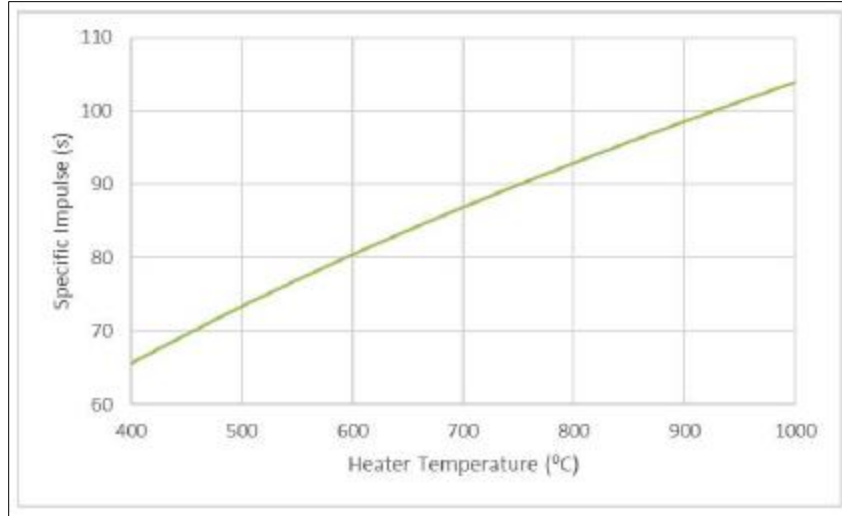


Figure 37. Expected Specific Impulse Performance of Resistojet Thruster [19]

While these expected performance levels for specific impulse for this thruster were low in comparison to some monopropellant thrusters, the thruster still held the massive advantages of toxic propellant avoidance and fairly low storage pressures. Furthermore, the expected performance for the thruster far exceeded that of typical cold-gas thrusters while maintaining a relatively high-density propellant storage. [19]

Along with expected performance levels for thrust and specific impulse, the paper discussed some additional impacts that were expected but unmodeled. Firstly, it was expected that the pressure drop across the 2 pairs of the propellant control valves was unlikely to be negligible. The internal geometry of these valves were also unknown and thus made it quite difficult to arrive at a prediction for this expected pressure drop. Direct measurement of this pressure drop was not possible either, thus resulting in a non-isolatable yet constant effect on the total pressure loss in the system. Secondly, it was expected that the pressure drop across the numerous bends and turns in the system was

also unlikely to be negligible. This included the path between the tank and the valves, the path between the two pairs of valves themselves, the path leading to the metering orifice, and the path within the heater block. The most latter path was expected to be particularly significant, as it held 38 180° turns and was also predicted to have rather rough wall passages. Specifically, it was expected there would be a 18-20 μm wall roughness accompanying the known 2 mm passage diameter, giving a relative roughness around 0.01 and a considerable friction factor. [19]

Finally, it was expected that the speeds within the heater block would reach over 100 m/s by the end of the path due to the combined impacts from viscous and thermal effects. Modeling this prediction directly was considered an extensive computational fluid dynamics problem that was outside the scope of this development. Instead, previous modeling was relied on to predict how this would affect performance. It was predicted that there would be a 90% pressure loss across the heater block due to friction as well as entropy gain from heating. [19]

IV. Analysis and Results

Chapter Overview

The purpose of this chapter is to outline the results of the water-propellant resistojet thruster assembly, the potential causes of these results, and the effects brought upon by these results. Furthermore, this chapter discusses the results of the heater block functional check achieved through direct propellant feed. Finally, this chapter also outlines the results of the measured heat losses occurring from the resistor component of the thruster.

Results of Thruster Assembly and Integration

While the thruster prototype used in the laboratory for testing was never intended as a flight model or as a fully operational demonstration, it was intended to demonstrate that the interim design was functional and performed at an expected level. For instance, while inert gas was pumped directly into the pressurant volume instead of using the proposed temperature manipulation of hexafluoropropane, the purposes of testing were focused on evaluating performance values such as thrust and specific impulse, not testing if the ideal gas law still holds true. Thus, certain liberties were taken to reduce complexities in assembly and integration and allow focus on the desired results, in this case, removing the variable of having to verify that the pressurant works as intended. Similar liberties can be said about the power and electrical aspects that occurred in the thruster testing environment.

Still, there were some components that were inadvertently brought along for testing as assembly and integration steered toward the goal of testing thruster

performance. While some components such as electrical interface and pressurant were substituted from what the flight design would operate off of, a certain point is reached where too many component substitutions begin to raise the inquiry of if the resistorjet thruster design itself is even being tested anymore. Thus, the electrical interface and pressurant remained the only initially planned component substitutions for testing purposes. By this, in the process of testing for thruster performance, testing is also done on the piston functionality, propellant control valve functionality, and more. Thus, any additional necessary component substitutions or alterations needed for testing are then considered a design failure or assembly failure. As discussed in Chapter 3, a variety of these failures were revealed.

The first of these failures was the incorrect, flipped installation of the propellant control valves onto the side of the thruster body. This failure affected operation of the thruster due to the fact that it negated the design of the propellant control valve layout that prevented single-point failures, and more so generally negated the overall ability to shut off thrust. Without the ability to shut off thrust, testing clearly would not be able to run successfully; the negation of the single-point failures became an afterthought as there was already a constant inherent failure. This failure occurred due to insufficient component literature review before assembly, as a simple examination of the component manual would have revealed the existence of a defined inlet and outlet. As mentioned in Chapter 3, there was no ability to directly correct the failure due to the seal of epoxy, and thus the solution was to modify the thruster assembly to accommodate the failure. Specifically, this took the form of an additional propellant control valve installed into the propellant flow path ahead of the failure, which would then be the primary location of

propellant flow control. This flipped control valve installation and the resulting additional control valve are shown below in Figure 38 and Figure 39.

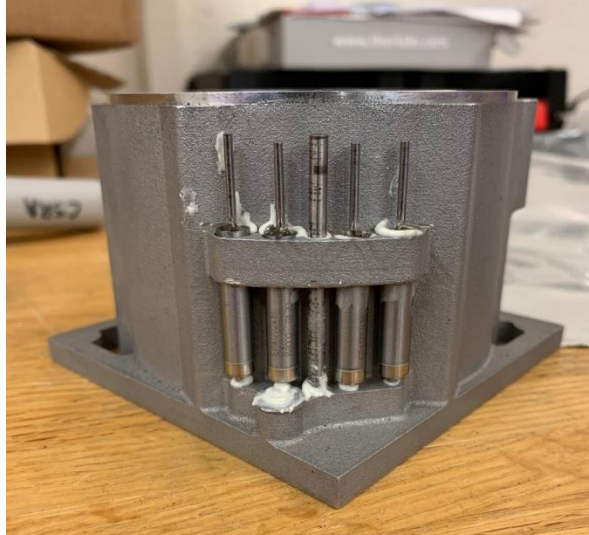


Figure 38. Control Valve Installation Failure

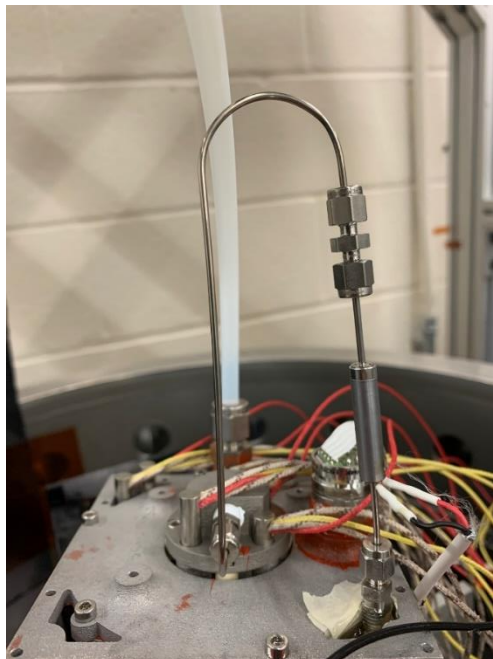


Figure 39. Corrective Control Valve

The second of these failures was the variety of faulty seals found around the thruster. Specifically, these were found in the O-rings sealing the top plate to the thruster body, and in the interfaces of the pressurant pressure sensor and pressurant fill port to the thruster top plate. This failure affected operation of the thruster due to the fact that without sufficient pressurant, there would be an inability to provide any meaningful thrust. Granted, this operational failure only applied to a situation where a future flight model is being tested, but the inability to hold pressurant still was considered a failure even with the thruster connected to an external gas tank for a separate reason. Even though the external gas tank would be able to maintain a constant pressure in the pressurant volume despite the leakage, this constant leakage diffusing into the vacuum chamber would have an effect on the thrust measurements.

As discussed in Chapter 2, the ambient pressure can affect the thrust provided by a rocket, and the constant pressurant leakage into the vacuum chamber would provide exactly this. A possible solution to this would be use of a roughing pump, but this introduces the chance of noise into the thrust measurements from the accompanying vibrations. Generally, this failure occurred due to the use of incorrectly sized O-rings and ineffective Teflon tape during assembly. As discussed in the previous chapter, the solution to this was simply application of room-temperature-vulcanizing silicone (RTV) into the O-ring interfaces and top plate interfaces. Still, while this limited the pressurant leak rate to an acceptable level for testing purposes, it is important to note that this leak rate was not nonexistent. The ineffective thread sealing through Teflon tape and the resulting solution through RTV are pictured below in Figure 40 and Figure 41.



Figure 40. Teflon Tape Sealing

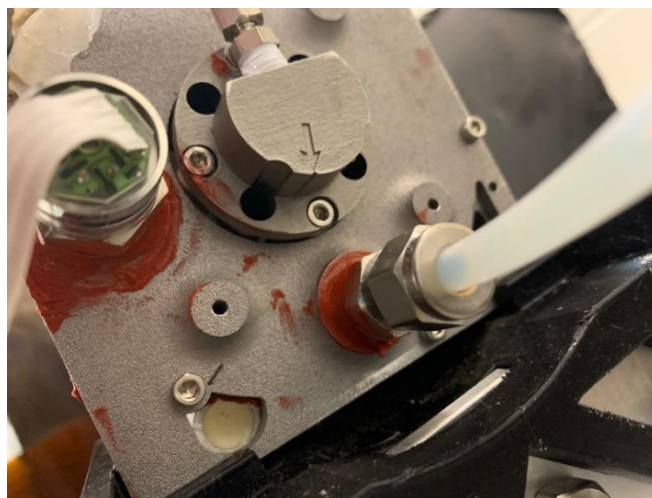


Figure 41. Corrective RTV Sealing

Additionally, the resulting RTV application to ensure a proper O-ring seal is pictured below in Figure 42.

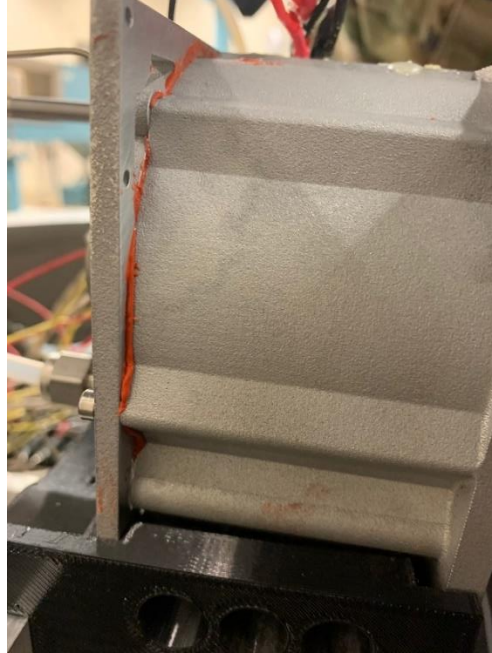


Figure 42. Corrective RTV Sealing

Finally, the third of these failures, and perhaps the most detrimental failure to occur during assembly, was the propellant leak found occurring from the propellant control valve manifold region. This failure affected operation of the thruster due to the fact that the leak was substantial enough to prevent propellant from entering the heater block. With propellant leaking off the side and not flowing through the heater block, there would be an inability by the resistojet to provide any meaningful thrust. Following, this would prevent any thrust measurements from being able to be taken and result in experiment failure.

As mentioned in Chapter 3, the later stages of thruster assembly were characterized by repeated leak fixes through application of epoxy, and thus, this failure is unique in that the direct cause was not identified immediately. While it was known there

was a propellant leak somewhere in the thruster, the exact location was not immediately known. In the effort to fix leaks by application of epoxy, it redirected propellant to appear as if the leak was occurring in a variety of different locations. But eventually, this epoxy application progressed to reveal that the leak was occurring from behind the manifold piece which connected the propellant control valves together in the flow path. After some deliberation, it was concluded that this leak was the result of a particular mistake made in the process of attempting to remedy a previous assembly failure.

During the attempt to fix the issue of pressurant leakage, as mentioned previously, RTV was applied to the O-ring interfaces to ensure a proper seal. During this RTV application, the top-sitting tube feature of the manifold was fractured from the rest of the manifold while attempting to separate the thruster top plate from the rest of the body. In the attempt to remedy this fracture, a separate piece of tubing was epoxied to the manifold and assumed to provide the same flow path integrity; this was not the case, and resulted in the aforementioned propellant leakage. This failure can be considered to be the most detrimental failure to occur during thruster assembly because there was no direct correction or assembly modification that could resolve the issue. With epoxy setting being a permanent modification, no method existed for removing the manifold and addressing the source of the leakage. With this failure, the overall thruster assembly resulted in a failure; the only way forward became to construct a new thruster with various design and assembly changes. Figure 43 below depicts the propellant control valve manifold installed into the flow path, with the top-sitting tube feature seen clearly; Figure 44 below depicts the attempted leakage fix through epoxy after the manifold fracture.



Figure 43. Installed Valve Manifold

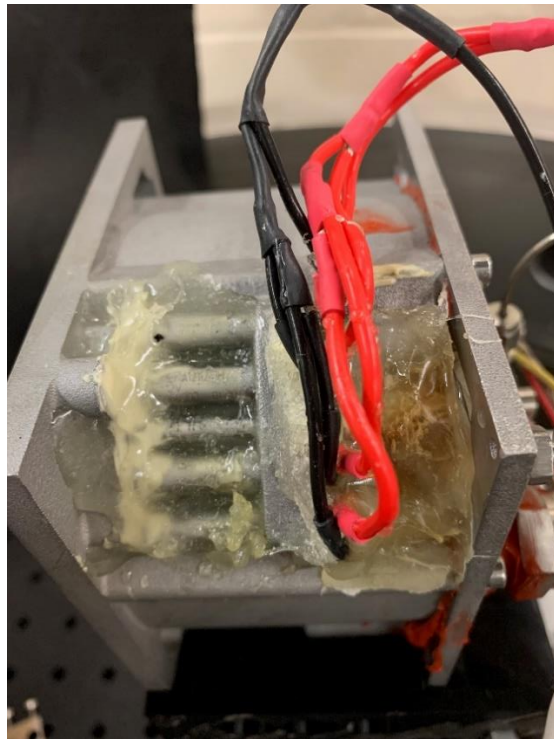


Figure 44. Epoxy Application

Results of Heater Block Functional Check

With the bypass of the propellant tank and control valve system, observation of an actual propulsive force became realizable. Still, this was achieved at the cost of the thruster itself not being fully tested, and instead only the heater block itself was tested. Furthermore, time constraints posed against the overall thruster research resulted in the inability to execute full performance testing on the heater block. Instead, only qualitative results and a general functional check of the heater block were realizable. Still, following the release of the inert gas, the functional check resulted in a successful flow of propellant through the heater block, the achievement of high-temperature steam, and an overall successful capability to produce an observable thrust. Pictured below in Figure 45 is a snapshot of the heater block producing this propulsive force.

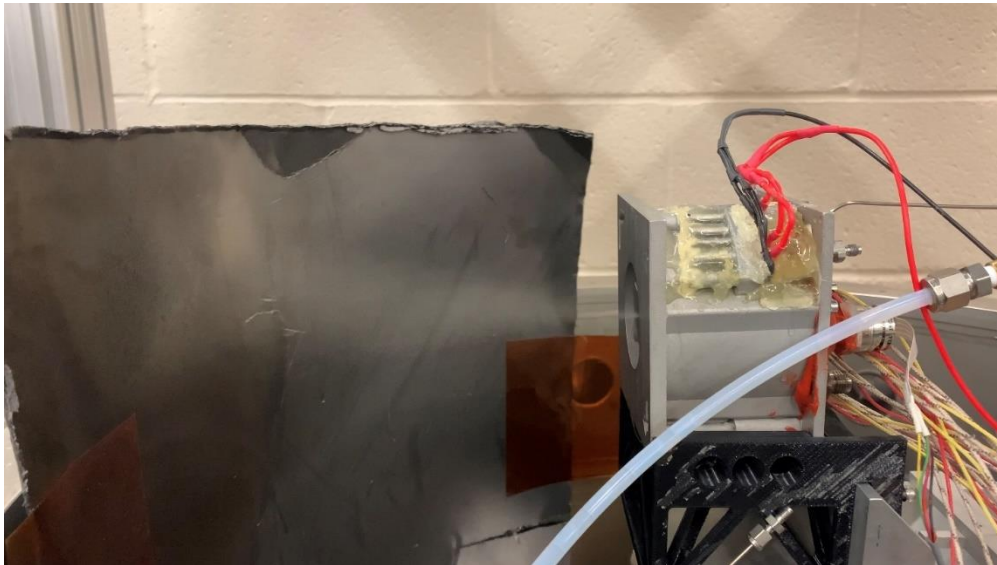


Figure 45. Observable Thrust

However, there was not a complete absence of drawbacks in the experiment. Not all air pockets were removed from the gas connection, and this resulted in sputtering as the thrust was produced. Still, this was a result of the connection setup and thus did not reflect on the functional performance of the heater block. Furthermore, with the experiment performed in an open chamber setting, the heater block did not achieve temperatures that fully converted all propellant to steam. This resulted in the occasional expulsion of liquid water, which was not desirable for producing meaningful thrust. Still, since the heater block would operationally perform in a vacuum, and thus achieve much higher temperatures, it was determined that this would not remain a potential future issue.

Results of Resistor Component Heat Losses

Following the tabulation of the temperature data from the heat loss experiment, the first step in analysis was the observation of any convective heat loss effects on the thruster. While the resistojet as a thruster is used exclusively in on-orbit operation, and thus will never encounter convective heat loss effects, this analysis provided comparative investigation of how the heater block performs in realistic vacuum conditions versus unrealistic atmospheric conditions. Essentially, this allowed for a depiction of why a vacuum chamber is a required testing condition and why atmospheric effects cannot be considered negligible. The effects of convective heat loss on the thruster could be seen upon first glance of the temperature data, which is given in Appendix A and Appendix B, as the final tank temperature showed a value of 347.04 K and 328.15 K for the open chamber and closed chamber experiments, respectively. Still, a more comprehensive analysis of these convective heat loss effects was desired, and thus enthalpy curves for

both the open chamber and closed chamber experiments were constructed. This was done by substituting certain properties of the Inconel 718 heater block in concert with the heat capacity equation, which is shown below in Equation 52. [25]

$$\Delta Q = mc\Delta T \quad (52)$$

where: $\Delta Q = \text{change in thermal energy [J]}$

$$m = \text{mass [kg]}$$

$$c = \text{specific heat } \left[\frac{\text{J}}{\text{kg} \cdot \text{K}}\right]$$

$$\Delta T = \text{change in temperature [K]}$$

With the two curves plotted for the heater block, the amount of heat lost to convective effects could be enumerated at any point in the experiment by finding the vertical difference in the two curves at a particular point. Notably, the final measurement for heat lost to convective effects was found to be 21.2 kJ. These results confirmed the significance of convective heat loss effects on the thruster, and that accurate resistor heat loss experimentation required testing within a vacuum environment. The plotted enthalpy curves are shown below in Figure 46.

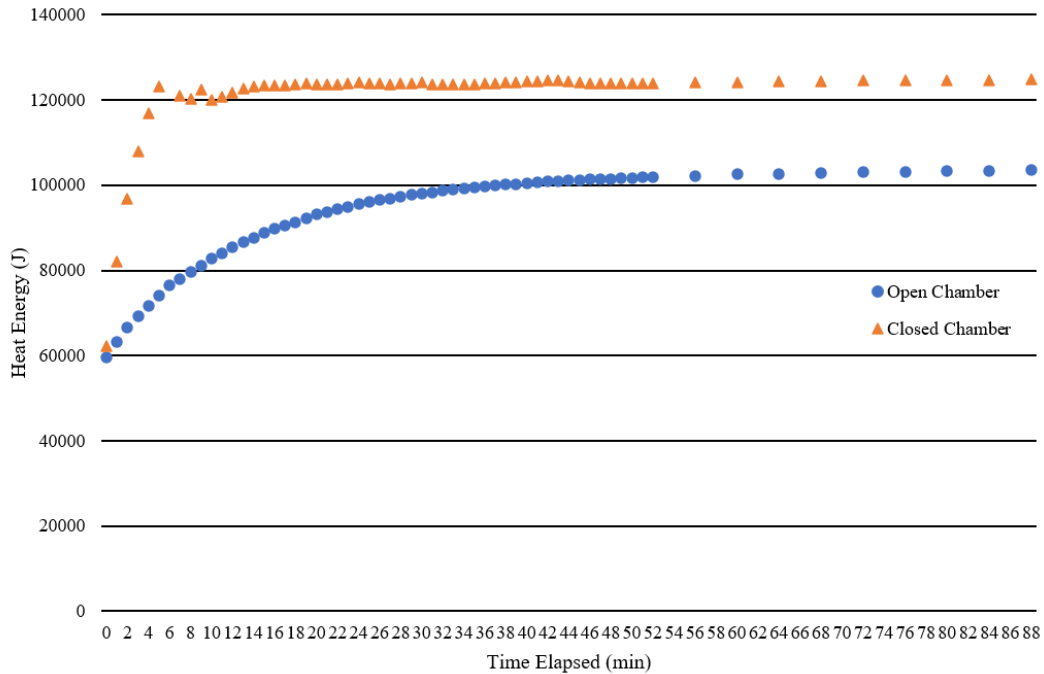


Figure 46. Heater Block Enthalpy Curves

Having the effects of convective heat loss enumerated, analysis of the raw temperature data for the closed chamber experiment could be performed. Immediately, it was clear that in vacuum, the heat radiated by the heater block was being effectively absorbed by the propellant tank, as the displayed tank temperature continued to rise for the entirety of the experiment. At the end of the experiment, the tank temperature had reached 328.15 K, which posed a design problem. Regarding the temperature-pressure curve for R-236fa, the chosen cutoff temperature that designated the inability to control the pressurant pressure was 50 °C, or 323.15 K.

With the propellant tank at such a temperature, conductive heat transfer would also raise the pressurant to a temperature of 328.15 K. Finding the final tank temperature value in the experiment to be 328.15 K, this confirmed that the current thruster design

would not be able to independently control the pressure of the pressurant given enough elapsed time. Even more so, this experiment was terminated at an arbitrary point before the tank temperature could fully rise; if the experiment were run for longer, the tank temperature would have risen even higher to be more than sufficient at destabilizing the pressurant. Plotted below in Figure 47 is the data of the tank temperature over time, seen continuously rising due to the absorbing of the heat radiated by the heater block.

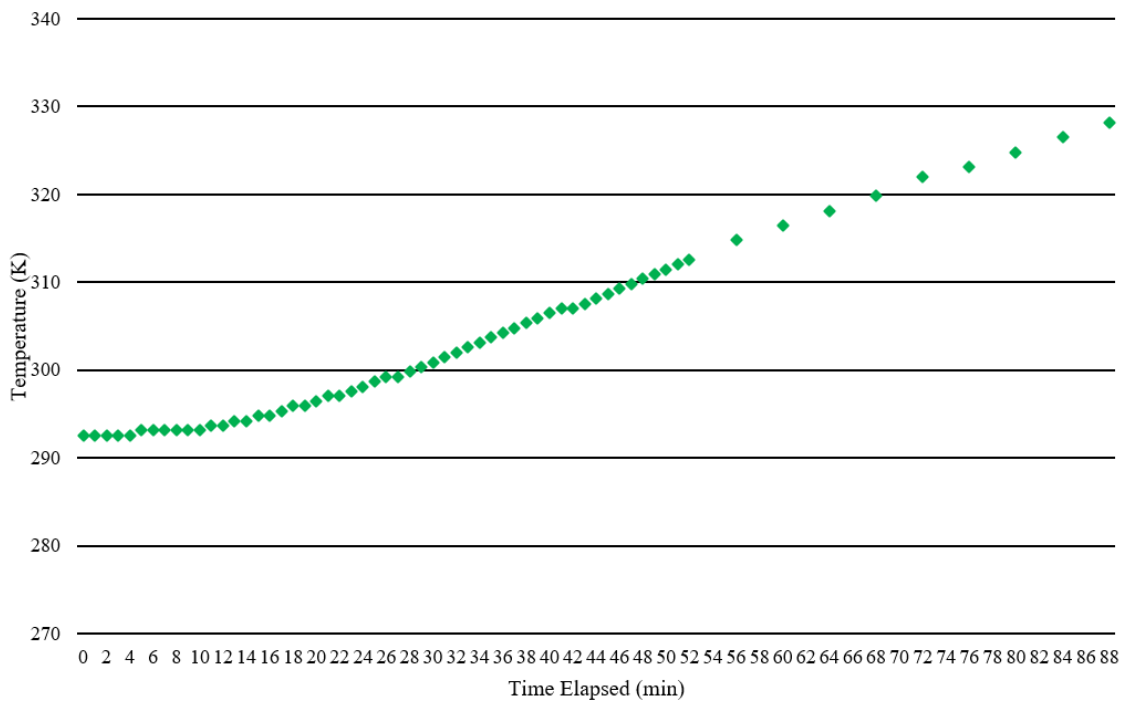


Figure 47. Tank Temperature

However, an unexpected finding in the experiment was the rapid rise in temperature of the heater block in the vacuum environment. While it was known that the heater block would reach high temperatures eventually, it was assumed that the time

required to achieve this would be somewhere shortly ahead of 60 minutes. Surprisingly, the heater block was able to reach temperatures near 800 °F in less than 5 minutes. Figure 48 below shows the temperature behavior of the heater block in the closed chamber environment, in the first 15 minutes of the experiment.

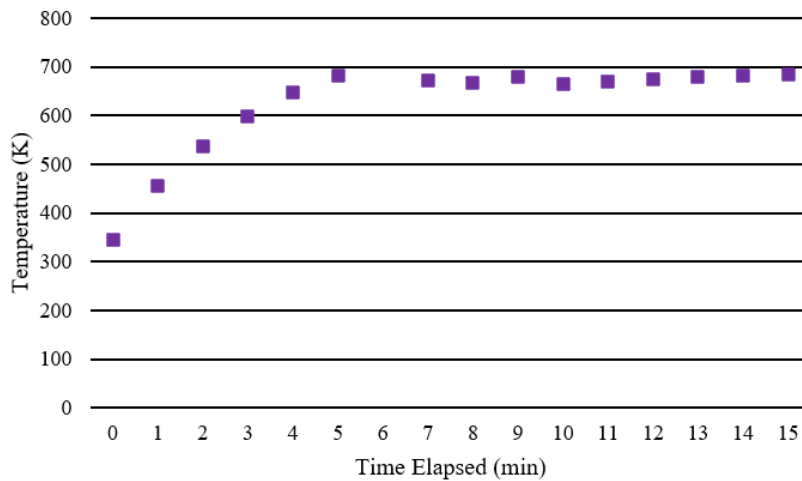


Figure 48. Initial Heater Block Temperature

This finding was significant because while the tank temperature did continue to rise throughout the experiment, it did so at a much lower rate compared to the heater block. This infers that if the heater block requires only 5 minutes to reach acceptable levels, the tank temperature will never reach levels high enough to destabilize the pressurant because there is simply not enough time to do so. Essentially, while the thruster is technically not able to independently control the pressure of the pressurant given enough elapsed time, this fact is trivial, because it will never reach the opportunity. Thus, operationally, the resistojet thruster would activate the resistive heater component merely 5 minutes before a scheduled firing, and the heat absorbed by the propellant tank would never reach a level of concern.

While the tabulated tank temperature data showed the changes in tank temperature over time, there was a desire to calculate the net total power being absorbed by the tank due to the assumed absence of a steady-state condition. This was achieved through use of an expanded form of the Stefan-Boltzmann Law, one which calculated power over an entire area and scaled to a corresponding emissivity.

$$P = A\varepsilon\sigma T^4 \quad (53)$$

where:

$$P = \text{total power [W]}$$

$$A = \text{surface area [m}^2\text{]}$$

$$\varepsilon = \text{emissivity [unitless]}$$

$$\sigma = 5.670374 \cdot 10^{-8} \left[\frac{W}{m^2 \cdot K^4} \right]$$

$$T = \text{temperature [K]}$$

However, the desired value was the net total power, and thus the power radiating from the tank needed to be considered as well. This introduced the consideration of multiple temperatures, but also the concept of view factors. Roughly, view factors are the ratio of field of view an object takes up as seen by a radiation source. Thus, if an object completely takes up the field of view of a radiation source, the view factor in the direction from the source to the object is 1.0; due to the design of the heater block and propellant tank geometry; this was the same case. Furthermore, the relationship between radiating surface areas and view factors can be described by Equation 54 given below.

$$A_1 F_{1 \rightarrow 2} = A_2 F_{2 \rightarrow 1} \quad (54)$$

Thus, if the surface areas of two radiating objects are known and the view factor in one direction is known, the view factor in the opposite direction can be solved for. This was the case for the thruster heater block and surrounding propellant tank, as approximate surface area measurements taken of the corresponding radiation surfaces revealed an A_1 , or A_{block} , of $8.20816 \cdot 10^{-3} \text{ m}^2$ and an A_2 , or $A_{innertank}$, of 0.01104 m^2 , and a $F_{1 \rightarrow 2}$ of 1.0, as mentioned previously. This gave a view factor $F_{2 \rightarrow 1}$ of 0.743, which revealed that only roughly 74% of the radiation emitting from the inner tank surface was impacting the heater block, an important factor in calculating the net total power.

Finally, since the heater block and surrounding propellant tank were made of differing materials, the consideration of multiple emissivity values were introduced into the calculation. While the specific emissivity values for each component were unknown, rough estimates could be made through reference of the previously researched emissivity values outlined in Chapter 2. For these calculation purposes, the emissivity values chosen were 0.28 for Inconel 718 and 0.222 for AlSi12 Aluminum Alloy, values which assumed the most emissive scenario. With this, the net total power being absorbed by the propellant tank could be calculated; this final calculation method is shown below in Equation 55.

$$P_{net\ 1 \rightarrow 2} = \varepsilon_1 A_1 \sigma F_{1 \rightarrow 2} (T_1^4) - \varepsilon_2 A_2 \sigma F_{2 \rightarrow 1} (T_2^4) \quad (55)$$

The appropriate values were substituted into the calculation, taking the temperature values to be the final values recorded in the experiment, and resulted in the net total power being absorbed by the tank to be found at 28.59 W. This posed an issue, as the input power into the heater block was only 20.6 W, thus resulting in a higher power out than power in, which was a violation of thermodynamics. After some

deliberation, it was concluded that perhaps the emissivity values referenced from Chapter 2 were not at all an accurate estimate for the different thruster components, and significantly more accurate values were needed to be determined. Still, this same mathematical development remained relevant as the eventual determination of accurate emissivity values would allow for insightful heat transfer analysis.

V. Conclusions and Recommendations

Chapter Overview

The purpose of this chapter is to present conclusions and discuss the significance of the research performed on the water-propellant resistojet thruster. Furthermore, this chapter discusses recommendations for future work to be performed on the thruster. Specifically, these recommendations discuss potential thruster design changes to be made as well as potential paths forward with regard to testing.

Conclusions of Research

Performance of the resistojet thruster remains yet to be characterized as actual thruster construction has revealed a multitude of both design flaws and assembly risks. While the inverted installation of the propellant control valves was an assembly failure, it has revealed a design flaw in the current manifold design housing the valve system; the correct installation of the propellant control valves is not possible in the current valve housing design. Furthermore, the resistojet thruster by design alone is not nearly gas-tight enough to allow for R-236fa to remain enclosed as a pressurant, and currently requires use of RTV to ensure proper seals. Most of all, structural integrity of the top-sitting tube section of the control valve flow path manifold must be maintained to ensure flow path integrity. Granted, the fracture of this manifold that led to unsolvable propellant leakage was purely an assembly failure, yet, it highlights a significant assembly risk of the thruster overall moving forward.

Conversely, the additively manufactured heater block is functionally viable and can provide an observable thrust given a pressurized propellant flow. The heater block

passages successfully convert the liquid propellant to steam, and the concluding nozzle successfully accelerates the outgoing flow. Lastly, heat loss experimental testing has shown that, detrimentally, the propellant tank is effectively absorbing heat radiated outward by the heater block. This has resulted in a continuous rise in the tank temperature over time, and while the experiment was concluded after 88 minutes, it is assumed that this temperature would continue to rise given additional time. However, this testing has also shown that the heater block temperatures are reaching significantly high levels extremely quickly, and thus the potential issue for pressurant destabilization caused by high tank temperatures is negated due to the sheer lack of time to achieve such effects.

Significance of Research

The significance of this research lies in the first realization of a simple idea into an initial prototype. Volumes of previous research done to design a CubeSat compatible 1U resistojet thruster, previous work done to obtain appropriate parts, and previous time spent constructing a 3D CAD model, all come together to this research, where the first attempt to bring a physical prototype to life is accomplished. While the results of this prototype ended as less than desirable, that in itself remains just as significant, as it provides a path forward for future research, and highlights the shortcomings that need to be solved for the next prototype. While new insight of the prototype was gained from the successful experimentation, perhaps even more insight was taken from the failures of the research.

Recommendations for Action

The primary recommendation for action towards the future research of the thruster is to construct a new, functional prototype. Due to the functional failure of the prototype constructed in this research arriving as a result of irreversible assembly failures, a completely new prototype must be constructed from scratch. Still, while construction of this new prototype will allow for the avoidance of the previously committed assembly failures, this new prototype must execute certain design changes based on the findings of this research. First, the propellant control valve housing manifold must be modified from a series of completely encapsulating rings to instead a series of slats. This is to allow the new, flipped, yet correctly installed, propellant control valves to slide down into the proper location. This must be done as the electrical prongs will not allow for installation unless the housing manifold is altered.

Furthermore, the O-ring interfaces that are designed to ensure a pressurant seal must be re-evaluated, or RTV must continue to be applied for every prototype. The current O-ring interface design does not effectively seal pressurant within the pressurant volume, and thus one of these two design paths must be selected. Finally, the idea of plating the exterior of the Inconel 718 heater block and the exterior, center-facing wall of the AlSi12 Aluminum Alloy propellant tank with a low-emissivity metal, such as gold, should be explored. While experimental testing showed that the radiated heat from the heater block would not pose a concern nominally, perhaps a thermal safeguard against a potential electrical failure, one where the resistor component cannot be shut off, would be beneficial.

Recommendations for Future Research

The primary recommendation for future research towards the thruster is to fully characterize the performance, evaluating levels for thrust and specific impulse for varying pulse durations. While this was included in the research objectives for this research, various design and assembly failures identified during thruster construction prevented this from ever coming to fruition, and thus still remains as a research objective. Furthermore, experimental testing should be performed to evaluate if a low-emissivity material plating is necessary as a thermal safeguard against runaway electrical failures, and how beneficial this plating would be to overall thruster function.

Appendix A: Open Chamber Experiment Data Table

Tank (°F)	Tank (K)	HB1 (°F)	HB1 (K)	HB2 (°F)	HB2 (K)	HB (Avg) (K)	Elapsed Time (min)
68	293	137	331	134	330	331	0
68	293	174	352	170	350	351	1
68	293	207	370	202	368	369	2
69	294	234	385	229	383	384	3
69	294	258	399	254	396	398	4
70	294	282	412	278	410	411	5
71	295	304	424	301	423	423	6
71	295	319	433	316	431	432	7
72	295	336	442	333	440	441	8
74	296	352	451	349	449	450	9
75	297	367	459	365	458	459	10
76	298	380	466	378	465	466	11
77	298	394	474	392	473	474	12
78	299	406	481	404	480	480	13
80	300	416	486	415	486	486	14
81	300	427	493	425	491	492	15
83	301	436	498	435	497	497	16
85	303	442	501	444	502	501	17
87	304	451	506	452	506	506	18
88	304	457	509	462	512	511	19

90	305	468	515	470	516	516	20
92	306	474	519	476	520	519	21
94	308	480	522	482	523	523	22
96	309	486	525	488	526	526	23
97	309	492	529	494	530	529	24
100	311	498	532	501	534	533	25
101	311	502	534	504	535	535	26
103	313	506	536	508	538	537	27
105	314	511	539	513	540	540	28
107	315	514	541	516	542	541	29
108	315	517	543	519	544	543	30
110	316	520	544	523	546	545	31
112	318	523	546	526	548	547	32
113	318	526	548	528	549	548	33
115	319	529	549	531	550	550	34
117	320	531	550	533	551	551	35
118	321	534	552	536	553	553	36
120	322	536	553	538	554	554	37
121	323	538	554	540	555	555	38
123	324	540	555	542	556	556	39
125	325	541	556	544	558	557	40
126	325	543	557	545	558	558	41
127	326	545	558	547	559	559	42

129	327	547	559	549	560	560	43
130	328	548	560	550	561	560	44
132	329	549	560	551	561	561	45
133	329	550	561	552	562	561	46
134	330	551	561	553	563	562	47
135	330	552	562	554	563	563	48
136	331	553	563	556	564	563	49
138	332	554	563	556	564	564	50
138	332	555	564	557	565	564	51
140	333	556	564	558	565	565	52
144	335	559	566	561	567	566	56
147	337	562	568	564	569	568	60
151	339	564	569	566	570	569	64
154	341	566	570	568	571	570	68
157	343	568	571	570	572	571	72
159	344	569	571	571	573	572	76
161	345	570	572	572	573	573	80
163	346	571	573	573	574	573	84
165	347	573	574	574	574	574	88

Appendix B: Closed Chamber Experiment Data Table

Tank (°F)	Tank (K)	HB1 (°F)	HB1 (K)	HB2 (°F)	HB2 (K)	HB (Avg) (K)	Elapsed Time (min)
67	293	162	345	159	344	345	0
67	293	359	455	360	455	455	1
67	293	503	535	508	538	536	2
67	293	611	595	623	601	598	3
67	293	699	644	714	652	648	4
68	293	763	679	777	687	683	5
68	293						6
68	293	741	667	756	675	671	7
68	293	734	663	745	669	666	8
68	293	757	676	767	681	679	9
68	293	733	663	741	667	665	10
69	294	742	668	747	670	669	11
69	294	753	674	757	676	675	12
70	294	762	679	765	680	680	13
70	294	768	682	771	684	683	14
71	295	770	683	774	685	684	15
71	295	771	684	774	685	685	16
72	295	771	684	774	685	685	17
73	296	773	685	775	686	685	18
73	296	775	686	776	686	686	19

74	296	773	685	773	685	685	20
75	297	774	685	773	685	685	21
75	297	775	686	774	685	686	22
76	298	777	687	775	686	686	23
77	298	779	688	777	687	688	24
78	299	778	688	775	686	687	25
79	299	777	687	774	685	686	26
79	299	777	687	773	685	686	27
80	300	778	688	773	685	686	28
81	300	779	688	774	685	687	29
82	301	780	689	775	686	687	30
83	301	777	687	772	684	686	31
84	302	777	687	770	683	685	32
85	303	777	687	770	683	685	33
86	303	777	687	770	683	685	34
87	304	778	688	771	684	686	35
88	304	779	688	772	684	686	36
89	305	780	689	773	685	687	37
90	305	782	690	774	685	688	38
91	306	783	690	775	686	688	39
92	306	784	691	776	686	689	40
93	307	786	692	777	687	690	41
93	307	787	693	779	688	690	42

94	308	788	693	780	689	691	43
95	308	785	691	777	687	689	44
96	309	783	690	775	686	688	45
97	309	781	689	773	685	687	46
98	310	780	689	772	684	686	47
99	310	780	689	772	684	686	48
100	311	780	689	772	684	686	49
101	311	779	688	772	684	686	50
102	312	779	688	772	684	686	51
103	313	780	689	772	684	686	52
107	315	781	689	774	685	687	56
110	316	782	690	775	686	688	60
113	318	784	691	777	687	689	64
116	320	785	691	778	688	690	68
120	322	786	692	780	689	690	72
122	323	788	693	781	689	691	76
125	325			783	690	690	80
128	326			784	691	691	84
131	328			785	691	691	88

Bibliography

- [1] K. S. Poniatowski, "NASA Secondary Payload Plans, Policies and Requirements," National Aeronautics and Space Administration, Washington, D.C., 1990.
- [2] Moog Incorporated, "Spacecraft Payload Interfaces," 2021. [Online]. Available: <https://www.moog.com/products/spacecraft-payload-interfaces.html>. [Accessed 1 April 2021].
- [3] Space Exploration Technologies Corporation, "SpaceX - Falcon 9," 2021. [Online]. Available: <https://www.spacex.com/vehicles/falcon-9/>. [Accessed 2 April 2021].
- [4] H. W. Jones, "The Recent Large Reduction in Space Launch Cost," in International Conference on Environmental Systems (ICES), Albuquerque, 2018.
- [5] G. Shotwell, Interviewee, Broadcast 2212: Special Edition, interview with Gwynne Shotwell. [Interview]. 21 March 2014.
- [6] J. Foust, "SpaceX Revamps SmallSat Rideshare Program," SpaceNews, p. 1, 29 August 2019.
- [7] A. Narune and E. Prasad, "Small Satellite Market Size, Growth, Forecast 2021-2027," Allied Market Research, 2019.
- [8] D. B. Tomlin, "Creation and Presentation of a Systems-Level Model for an AF-M315E Monopropellant Micro-Thruster," Journal of DoD Research and Engineering, p. 12, 2018.
- [9] J. D. C. de La Harpe, "Performance Characterization of a Novel Plasma Thruster to Provide a Revolutionary Operationally Responsive Space Capability with Micro- and Nano-Satellites," Journal of DoD Research and Engineering, 2011.
- [10] G. Sowers, "Space Resources and the Cislunar Propellant Economy," Colorado School of Mines, Golden, 2021.
- [11] G. P. Sutton and O. Biblarz, Rocket Propulsion Elements, 9th ed., Hoboken: John Wiley & Sons Incorporated, 2017.

- [12] A. Karabeyoglu, "Lecture 2: Thrust Equation, Nozzles, and Definitions," Stanford University, Palo Alto, 2019.
- [13] National Aeronautics and Space Administration, "Nozzle Design - Converging/Diverging (CD) Nozzle," 5 May 2015. [Online]. Available: <https://www.grc.nasa.gov/www/k-12/airplane/nozzled.html>. [Accessed 23 April 2021].
- [14] R. G. Jahn, Physics of Electric Propulsion, Mineola: Dover Publications Incorporated, 2006.
- [15] F. P. Incropera, D. P. Dewitt, T. L. Bergman and A. S. Lavine, Fundamentals of Heat and Mass Transfer, Hoboken: John Wiley & Sons, Incorporated, 2007.
- [16] R. W. Humble, G. N. Henry and W. J. Larson, Space Propulsion Analysis and Design, New York: The McGraw-Hill Companies, Incorporated, 1995.
- [17] National Aeronautics and Space Administration, "Equation of State," 7 May 2021. [Online]. Available: <https://www.grc.nasa.gov/www/k-12/airplane/eqstat.html>. [Accessed 12 May 2021].
- [18] D. Roylance, "Pressure Vessels," Massachusetts Institute of Technology, 23 August 2001. [Online]. Available: <https://web.mit.edu/course/3/3.11/www/modules/pv.pdf>. [Accessed 12 May 2021].
- [19] C. Hartsfield, T. Shelton and G. Cobb, "Design of a High Reliability Compact CubeSat Propulsion System," in SciTech Forum, Virtual Event, 2021.
- [20] C. D. Tommila, C. R. Hartsfield, J. J. Redmond, J. R. Komives and T. E. Shelton, "Performance Impacts of Metal Additive Manufacturing of Very Small Nozzles," American Society of Civil Engineers, Reston, 2021.
- [21] J. H. Lienhard IV and J. H. Lienhard V, A Heat Transfer Textbook, Fifth ed., Cambridge: Phlogiston Press, 2020.

- [22] B. P. Keller, S. E. Nelsom, K. L. Walton, T. K. Ghosh, R. V. Tompson and S. K. Loyalka, "Total hemispherical emissivity of Inconel 718," *Nuclear Engineering and Design*, vol. 287, 2015.
- [23] Yang, Gu, Dai and ma, "Laser energy absorption behavior of powder particles using ray tracing method during selective laser melting additive manufacturing of aluminum alloy," *ResearchGate*, April 2018. [Online]. Available: https://www.researchgate.net/publication/323237520_Laser_energy_absorption_behavior_of_powder_particles_using_ray_tracing_method_during_selective_laser_melting_additive_manufacturing_of_aluminum_alloy. [Accessed 5 October 2021].
- [24] G. K. Stefansson, "MLI Blankets," Penn State University, 29 September 2014. [Online]. Available: <https://hpf.psu.edu/2014/09/29/mli-blankets/>. [Accessed 6 October 2021].
- [25] R. G. Brown, "First Law of Thermodynamics Summary," Duke University, 12 April 2004. [Online]. Available: <https://webhome.phy.duke.edu/~rgb/Class/phy51/phy51/node59.html>. [Accessed 25 October 2021].

REPORT DOCUMENTATION PAGE			<i>Form Approved OMB No. 074-0188</i>		
<p>The public reporting burden for this collection of information is estimated to average 1 hour per response, including the time for reviewing instructions, searching existing data sources, gathering and maintaining the data needed, and completing and reviewing the collection of information. Send comments regarding this burden estimate or any other aspect of the collection of information, including suggestions for reducing this burden to Department of Defense, Washington Headquarters Services, Directorate for Information Operations and Reports (0704-0188), 1215 Jefferson Davis Highway, Suite 1204, Arlington, VA 22202-4302. Respondents should be aware that notwithstanding any other provision of law, no person shall be subject to a penalty for failing to comply with a collection of information if it does not display a currently valid OMB control number.</p> <p>PLEASE DO NOT RETURN YOUR FORM TO THE ABOVE ADDRESS.</p>					
1. REPORT DATE (DD-MM-YYYY) 23-12-2021		2. REPORT TYPE Master's Thesis		3. DATES COVERED (From – To) March 2021 – December 2021	
TITLE AND SUBTITLE Design and Performance Characterization of a Water-Propellant Resistojet Thruster			5a. CONTRACT NUMBER		
			5b. GRANT NUMBER		
			5c. PROGRAM ELEMENT NUMBER		
			5d. PROJECT NUMBER		
6. AUTHOR(S) Weathersby, Sean M., Second Lieutenant, USAF			5e. TASK NUMBER		
			5f. WORK UNIT NUMBER		
			8. PERFORMING ORGANIZATION REPORT NUMBER AFIT-ENY-MS-21-D-077		
7. PERFORMING ORGANIZATION NAMES(S) AND ADDRESS(S) Air Force Institute of Technology Graduate School of Engineering and Management (AFIT/EN) 2950 Hobson Way, Building 640 WPAFB OH 45433-7765					
9. SPONSORING/MONITORING AGENCY NAME(S) AND ADDRESS(ES) Intentionally left blank			10. SPONSOR/MONITOR'S ACRONYM(S)		
			11. SPONSOR/MONITOR'S REPORT NUMBER(S)		
12. DISTRIBUTION/AVAILABILITY STATEMENT DISTRUBTION STATEMENT A. APPROVED FOR PUBLIC RELEASE; DISTRIBUTION UNLIMITED.					
13. SUPPLEMENTARY NOTES This material is declared a work of the U.S. Government and is not subject to copyright protection in the United States.					
14. ABSTRACT Secondary payloads, such as CubeSats, are being increasingly used by the US Department of Defense in the role of defense capability enhancement, and these increasingly complex defense missions can require extended lifespans that result in the need for a thruster. While many thruster options exist, characteristics such as propellant toxicity, complexity, and low performance limit many viable solutions. However, a potential answer that satisfies these thruster limitations is found in electrothermals, specifically the resistojet. The research presented here represents the first attempt to construct a 1U water-propellant resistojet thruster design and establish an initial characterization through evaluation of various performance values and design effects. This was achieved through assembly of additively-manufactured and commercial-off-the-shelf components, as well as construction and use of a vacuum chamber testing bed. This study revealed various inherent assembly risks and design flaws that resulted in the failure of the thruster to enter performance testing, yet heater block functionality was verified and heat loss experimental testing revealed how the design effects result in the propellant tank absorbing detrimental levels of heat over time. Still, due to the rapid function of the heater block, it was determined that this would not pose an operational issue in the future.					
15. SUBJECT TERMS resistojet, water-propellant, characterization, design, performance					
16. SECURITY CLASSIFICATION OF:			17. LIMITATION OF ABSTRACT UU	18. NUMBER OF PAGES 132	19a. NAME OF RESPONSIBLE PERSON Dr. Carl Hartsfield, AFIT/ENY
a. REPORT U	b. ABSTRACT U	c. THIS PAGE U			19b. TELEPHONE NUMBER (Include area code) (937) 255-6565, ext 4753 carl.hartsfield@afit.edu

